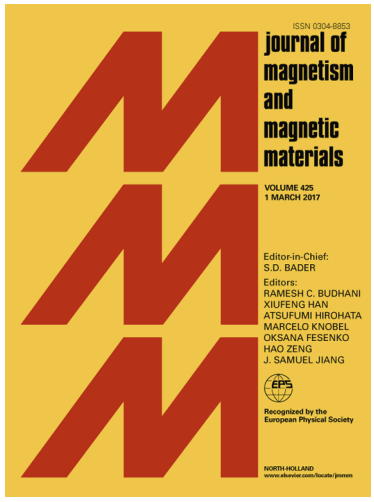

Structure, Non-stoichiometry, Valence of Ions, Dielectric and Magnetic Properties of Single-Phase $Bi_{0.9}La_{0.1}FeO_{3-\delta}$ Multiferroics

A.V. Pashchenko, N.A. Liedienov, Quanjun Li, D.D. Tatarchuk, V.A. Turchenko, I.I. Makoed, V.Ya. Sycheva, A.V. Voznyak, V.P. Kladko, A.I. Gudimenko, Y.V. Didenko, A.T. Kozakov, G.G. Levchenko

PII: S0304-8853(19)30475-5
DOI: https://doi.org/10.1016/j.jmmm.2019.03.095
Reference: MAGMA 65110

To appear in: *Journal of Magnetism and Magnetic Materials*

Received Date: 6 February 2019
Revised Date: 13 March 2019
Accepted Date: 21 March 2019

Please cite this article as: A.V. Pashchenko, N.A. Liedienov, Q. Li, D.D. Tatarchuk, V.A. Turchenko, I.I. Makoed, V.Ya. Sycheva, A.V. Voznyak, V.P. Kladko, A.I. Gudimenko, Y.V. Didenko, A.T. Kozakov, G.G. Levchenko, Structure, Non-stoichiometry, Valence of Ions, Dielectric and Magnetic Properties of Single-Phase $Bi_{0.9}La_{0.1}FeO_{3-\delta}$ Multiferroics, *Journal of Magnetism and Magnetic Materials* (2019), doi: https://doi.org/10.1016/j.jmmm.2019.03.095

Structure, Non-stoichiometry, Valence of Ions, Dielectric and Magnetic Properties of Single-Phase $Bi_{0.9}La_{0.1}FeO_{3-\delta}$ Multiferroics

A.V. Pashchenko[1,2,3,4,5], N.A. Liedienov[1,2,3,*], Quanjun Li[1], D.D. Tatarchuk[6], V.A. Turchenko[7], I.I. Makoed[8], V.Ya. Sycheva[9], A.V. Voznyak[5], V.P. Kladko[10], A.I. Gudimenko[10], Y.V. Didenko[6], A.T. Kozakov[11], G.G. Levchenko[1,2,3,*]

[1] *State Key Laboratory of Superhard Materials of Jilin University, 130012 Changchun, China*
[2] *International Center of Future Science of Jilin University, 130012 Changchun, China*
[3] *Donetsk Institute for Physics and Engineering named after O. O. Galkin, NASU, 03028 Kyiv, Ukraine*
[4] *Institute of Magnetism of NASU and MESU, 03142 Kyiv, Ukraine*
[5] *Donetsk National University of Economy and Trade named after Michael Tugan - Baranovsky, MESU, 50005 Kryvyi Rih, Ukraine*
[6] *National Technical University of Ukraine "Igor Sikorsky KPI", 03056 Kyiv, Ukraine*
[7] *Joint Institute for Nuclear Researches, 141980 Dubna, Russia*
[8] *A. S. Pushkin Brest State University, 224016 Brest, Belarus*
[9] *Donetsk Institute for Physics and Engineering named after O. O. Galkin, Donetsk, Ukraine*
[10] *V.E. Lashkaryov Institute of Semiconductor Physics, NASU, 03028 Kyiv, Ukraine*
[11] *Scientific-Research Institute of Physics at Southern Federal University, 344194 Rostov-na-Donu, Russia*

* Corresponding author
E-mail address: nikita.ledenev.ssp@gmail.com (N.A. Liedienov)
g-levch@ukr.net (G.G. Levchenko)

Abstract

The structure, microstructure, valence states, non-stoichiometry, dielectric and magnetic properties of lanthanum-modified multiferroics have been studied by X-ray diffraction, thermogravimetric, iodometric titration, SEM, XPS, dielectric spectroscopy and magnetic methods. Multiferroics of bismuth ferrite have been obtained by a rapid liquid phase sintering method under different pressures, *P*, for compacting stoichiometric mixture of precursors. On the basis of the experimental data, the molar formulas of real $BiFeO_{3-\delta}$ and $Bi_{0.9}La_{0.1}FeO_{3-\delta}$ structures have been determined. The real structure contains Bi^{3+}, La^{3+}, Fe^{3+}, Fe^{2+} and O^{2-} ions as well as cation $V^{(c)}$ and anion $V^{(a)}$ vacancies. The optimal temperature regimes of the rapid liquid phase sintering method for obtaining the single-phase $Bi_{0.9}La_{0.1}FeO_{3-\delta}$, whose composition corresponds to the concentration region of destruction of a spin cycloid, have been defined. It has been established that oxygen non-stoichiometry δ and concentration of Fe^{2+} strongly depend on the pressure *P*. The initial dielectric permittivity of the $Bi_{0.9}La_{0.1}FeO_{3-\delta}$ multiferroics can be controlled and changed by the pressure *P* more than 5000 times. The correlations between the composition, structure, non-stoichiometry, dielectric and magnetic properties in the $BiFeO_{3-\delta}$ and $Bi_{0.9}La_{0.1}FeO_{3-\delta}$ have been established. In the pure $BiFeO_{3-\delta}$ at room temperature, rhombohedral distortions of a hexagonal structure with indications of a ferromagnetic double exchange have been detected. The magnetic structure of the single-phase $Bi_{0.9}La_{0.1}FeO_{3-\delta}$ is homogeneous with a large value of coercitivity, $H_C \geq 10$ kOe, at room temperature. An analysis of the magnetic properties indicates the appearance of a weak ferromagnetism due to the destruction of the spin cycloid by lanthanum ions.

Keywords: multiferroics, non-stoichiometry, XPS, dielectric permittivity, coercitivity, ferromagnetic double exchange

1. Introduction

Bismuth ferrite, $BiFeO_3$, is a multiferroic and has a great prospect of its application in electronics and spintronics [1–3]. The uniqueness of the functional properties of the $BiFeO_3$ is associated to the possibility of the appearance of magnetoelectric [4], magnetocaloric [5], magnetodielectric [6], magnetostriction [7], piezoelectric [8], pyroelectric [9], and other galvanomagnetic effects in them, the coexistence of which is due to the structural, electrical and magnetic features of this metal oxide class.

The crystal lattice of the $BiFeO_3$ has a hexagonal ABO_3 perovskite structure with a rhombohedral $R3c$ type of elementary cell distortion [10], which is thermodynamically stable at room temperature. In the $BiFeO_3$, large bismuth cations occupy *A*-positions. Small iron cations occupy *B*-positions and form the FeO_6 octahedra with the coordination number (CN) = 6. The appearance of electric polarization in the $BiFeO_3$ is associated to a rhombohedral distortion of the ideal cubic perovskite lattice at which rotation of two adjacent FeO_6 octahedra around an [111] axis is occurred in an anti-phase regime [11]. The appearance of the electric polarization vector at such deformation of a crystal is associated to moving oxygen ions in a (111) plane towards the [111] axis in one part of the octahedron and from the [111] axis in the other part of the octahedron. As shown in [12], the angles of rotation of the two adjacent FeO_6 octahedra around the [111] axis are ± 13.8°. At this rotation, the polarization vector along the [111] direction can be changed from 6.1 μC/cm^2 for a bulk single crystal to 100 μC/cm^2 for a thin $BiFeO_3$ film [13,14]. The above mechanism for appearance of electric polarization allows to assume that a deviation from stoichiometry δ in the $BiFeO_{3-\delta}V_\delta$ perovskite, associated with appearance of point defects of the vacancy type V, can cause not only local distortions of the FeO_6 octahedra, but also significant changes in electric polarization towards either its reduction or increase. Therefore, the study of influence of non-stoichiometry and defect chemistry of a vacancy type on the structure and properties of the bismuth ferrite is of particular interest both to determine the conditions of the stable state for a single-phase multiferroic and to improve its functional properties.

The coexistence of magnetic and electrical ordering in the $BiFeO_3$ is due to the fact that this composition at room temperature is simultaneously in both antiferromagnetic (AFM) and ferroelectric

states with Neel of T_N ~ 650 K and Curie of T_C ~ 1100 K temperatures [15], respectively. The coexistence and mutual influence of the magnetic and electronic subsystems in the $BiFeO_3$ explains the appearance of galvanomagnetic effects, one of which is a magnetoelectric (ME) effect [16]. The appearance of a magnetic order below T_N is associated to AFM ordering of magnetic moments of iron. The appearance of uncompensated antiferromagnetism is a result of the appearance of a canted state in AFM lattice due to Dzyaloshinskii-Moriya interaction [17]. According to the high-resolution neutron powder diffraction data [18], the magnetic $BiFeO_3$ structure is spatially modulated since AFM ordered spins of Fe^{3+} form a spin cycloid with a period which increases from 605 to 625 Å with increasing temperature from 4 to 300 K. Since the spin cycloid exists, the average value of a projection of AFM magnetization vector in towards of a magnetic field is zero and there is no linear ME effect. This strongly limits the ability to use the unique properties of the $BiFeO_3$ multiferroics for application purposes. The cycloid structure in the $BiFeO_3$ can be destroyed by a strong magnetic field $H \approx 200$ kOe [19], which is accompanied by a surge of electric polarization and the appearance of the linear ME effect [20]. The destruction of the spin cycloid and the appearance of the linear ME effect are also observed in the thin films [21], and bismuth nanopowders with a nanoparticle size not exceeding the spin cycloid period of ~ 620 Å [22].

The appearance of the linear ME effect in weak magnetic fields can be also induced by chemical substitution of the *A*-cation. According to the Mössbauer spectroscopy data [23], the substitution of Bi^{3+} for La^{3+} ions in the $Bi_{1-x}La_xFeO_3$ destroys a cycloidal antiferromagnetism at the concentrations of $x \geq 0.2$. Measurements of hysteresis loops $M(H)$ in a magnetic field up to 7 T were showed that the residual magnetization in the $Bi_{1-x}La_xFeO_3$ increases from $5 \cdot 10^{-4}$emu/g to 0.13 emu/g with an increase in the concentration of lanthanum x from 0 to 0.05 [24]. Since the concentration $x = 0.1$ is in the boundary region of the appearance of the linear ME effect, an increased interest in a comprehensive study of the properties for the $Bi_{0.9}La_{0.1}FeO_3$ arises.

For obtaining large values of the ME effect in the multiferroics, it is necessary to have high polarization properties. The quantitative characteristic of polarization for the multiferroics is a dielectric

permittivity ε′, which dependents on a frequency and can take values from $\varepsilon' \sim 10^4$ in low frequency (LF) f = 1 Hz – 1 MHz to $\varepsilon' \sim 12$ in ultra high frequency (UHF) f = 8 – 12GHz ranges for the $BiFeO_3$ [25,26].

The complexity of the obtaining single-phase $BiFeO_3$ multiferroics is associated to the features of the Bi_2O_3-Fe_2O_3 state diagram [27]. Obtaining the $BiFeO_3$ by the solid state reaction method is a complex task which can be solved only within a narrow range of temperatures, compositions, and oxygen pressure [28]. In a state of stable equilibrium, three intermediate phases coexist: (i) the $BiFeO_3$ multiferroic with a perovskite structure; (ii) a $Bi_{25}FeO_{40}$ phase with a sillenite structure; and (iii) a $Bi_2Fe_4O_9$ bismuth ferrite with a mullite structure. The availability of the impurity $Bi_{25}FeO_{40}$ and $Bi_2Fe_4O_9$ phases leads to the appearance of a leakage current and degrades the functional properties of the $BiFeO_3$ [29]. Obtaining the single-phase $BiFeO_3$ is complicated by a volatility of bismuth above the melting point of 817 °C for a Bi_2O_3 oxide and thermodynamic instability of the $BiFeO_3$ in the air [30]. Using high temperature X-ray diffraction and isothermal heat treatment methods [31], the temperature effect on the thermodynamic stability of the $BiFeO_3$ was investigated and it was found out that the appearance and increase in the concentration of the second $Bi_{25}FeO_{40}$ and $Bi_2Fe_4O_9$ phases were observed within the temperature range of 600 – 817 °C. In the temperature range from 817 to 926 °C, the $BiFeO_3$ perovskite is a thermodynamically stable. Therefore, for obtaining the single-phase $BiFeO_3$ it is necessary to rapidly heat the stoichiometric Bi_2O_3-Fe_2O_3 mixture up to the synthesis temperature to prevent the formation of the $Bi_{25}FeO_{40}$ and $Bi_2Fe_4O_9$ phases, and at the final stage of the synthesis, the obtained $BiFeO_3$ perovskite needs to be rapidly cooled to prevent its decomposition into the $Bi_{25}FeO_{40}$, $Bi_2Fe_4O_9$ and Bi_2O_3. A rapid liquid phase sintering (RLS) method satisfies these conditions [32,33]. In the RLS method, the synthesis of the $BiFeO_3$ occurs at temperatures slightly above the melting point t = 817 °C of the low-melting component of Bi_2O_3. The process of mutual diffusion is much more intensively due to the higher transfer rate of the substance in a liquid phase. Such sintering is several minutes unlike solid state reaction synthesis with tens of hours. Using the RLS method allows to obtain the single-phase compositions of bismuth ferrite multiferroics in a record short time.

In an ideal $BiFeO_3$ perovskite structure, ions of bismuth, iron, and oxygen are in the valence states of Bi^{3+}, Fe^{3+} and O^{2-}. A real perovskite structure is defective and contains vacancies which strongly affect the physical properties of this metal oxide class [34]. As shown in [35], the perovskite structure can contain point defects of a vacancy type not only in an anion, but in a cation sublattice as well. At studying the effect of vacancies on the electrical properties of the $BiFeO_3$ multiferroics [36], a domain wall appears in the agglomeration region of cation $V^{(c)}$ vacancies in the *A*-positions of bismuth, when a domain structure of the ferroelectric state is formed.

Bismuth in the $BiFeO_3$ multiferroic can have Bi^{3+} and Bi^{5+} valence with a valence electron configuration $5d^{10}6s^2$ and $5d^{10}$, respectively. Bismuth ions do not contribute to the magnetization of the $BiFeO_3$ since their electron shells are completely filled and the total spin of the ion is zero. According to the X-ray photoelectron spectroscopy (XPS) data [37], the valence of bismuth is Bi^{3+} in the single-phase $BiFeO_3$ perovskite, and Bi^{5+} appears in impurity phase of $Bi_{24}^{3+}[Bi^{5+}Fe^{3+}]O_{40}^{2-}$ sillenite.

The deviation from stoichiometry in an oxygen sublattice of the $BiFeO_3$ leads to a decrease in its negative charge by anion $V^{(a)}$ vacancies, which is compensated by the appearance of Fe^{2+}. According to the results of XPS analysis [38], iron ions can be in Fe^{2+} state up to 28% in $BiFeO_3$. With the appearance of Fe^{2+}, an increase in conductivity and dielectric loss as well as a decrease in electrical polarization and dielectric constant are observed [38]. Taking into account the local reduction of the CN from 6 to 4 in the *B*-position by the $V^{(a)}$, it allows to assume that not only FeO_6 octahedra, but also FeO_4 tetrahedra exist. In this case, Fe^{3+} ions can be found both in the FeO_6 octahedra and FeO_4 tetrahedra, and Fe^{2+} are only in the FeO_6 octahedra [39]. Such effect of the non-stoichiometry on the change in the valence state and coordination environment of iron should cause a change in the formation of magnetic and conductive properties of the $BiFeO_3$.

Taking into account the non-stoichiometry and the possible valence state of the ions in the replaced $Bi_{1-x}La_xFeO_3$, the molar formula of its real structure is $\{Bi_{1-x'-x}^{3+}Bi_{x'}^{5+}V_x^{(c)}\}_A[Fe_{y'}^{2+}Fe_{1-y'-y}^{3+}V_y^{(c)}]_B O_{3-\delta}V_\delta^{(a)}$, where x and y are the concentration of the cation $V^{(c)}$ vacancies in the *A*- and *B*-sublattices, x' and y' are the concentration of Bi^{5+} and Fe^{2+}, δ is the number of

the anion $V^{(a)}$ vacancies per molar formula, the concentration of which equals to δ/3. The problem determining the type and concentration of point defects is an important task in chemistry, physics and engineering of functional materials.

Taking into account the above mentioned, the main tasks of this work can be formulated:

(i) obtaining the bismuth ferrite $Bi_{1-x}La_xFeO_3$ multiferroic, whose composition with lanthanum concentration of $x = 0 – 0.1$ is located in the region of destruction of the spin cycloid;

(ii) determining the optimal conditions for the preparation of the single-phase $Bi_{0.9}La_{0.1}FeO_3$ multiferroics by the RLS method;

(iii) defining the molar formulas of the real $\{Bi^{3+}_{1-x'-x}Bi^{5+}_{x'}V^{(c)}_x\}_A[Fe^{2+}_{y'}Fe^{3+}_{1-y'-y}V^{(c)}_y]_BO_{3-\delta}V^{(a)}_\delta$ structure containing different valence bismuth and iron ions as well as anion $V^{(a)}$ and cation $V^{(c)}$ vacancies;

(iv) studying the structure, dielectric and magnetic properties of the $Bi_{0.9}La_{0.1}FeO_{3-\delta}$ with establishing regularities of the influence of composition, non-stoichiometry and structure on these properties.

2. Experimental section

The ceramic $BiFeO_3$ and $Bi_{0.9}La_{0.1}FeO_3$ samples were prepared by the RLS method. A mixture of high purity La_2O_3 (≥ 99.5%), Bi_2O_3 (≥ 99.5%) and Fe_2O_3 (≥ 99.5%) powders in a stoichiometric ratio was calcined at 180 °C (4 h) for dehydration and pressed into tablets (Ø = 8 mm, h = 3 mm) under pressure P = 200 MPa and (Ø = 6 mm, h = 3 mm) under P = 400 MPa. The obtained samples were sintered in the air at a temperature of t_{ann} = 850 ºC for 480 sec in the mode of rapid heating at a speed of 100 °C/sec in a temperature range from a room temperature to 770 °C and at a speed of 10 °C/min in the range from 770 to 850 °C. After sintering, the samples were rapidly cooled from 850 to a room temperature at a rate of 100 °C/sec. Two batches of the samples were obtained, which were different by P = 200 and 400 MPa of the initial mixture of powders.

The symmetry, lattice parameters and phase composition were measured by using PANalitical X-Pert PRO MRD high resolution diffractometer in Cu$K_{\alpha1}$-radiation. Qualitative phase analysis was performed using database ICDD, PDF-2 Release 2012 and Crystallographica Search-Match Version 3, 1,

0, 0 software. The concentration of available phases was evaluated by the corundum numbers method [40]. Additional studies of temperature dependences of lattice parameters for the $Bi_{0.9}La_{0.1}FeO_3$ were performed by Empyrean X-ray diffractometer (PANalytical) in Cu-radiation. Low-temperature studies of the crystal structure were carried out in the temperature range from 18 to 290 K with using a closed cycle refrigerator and a low temperature Phenix X-ray prefix from Oxford Cryosystems. The analysis of experimental data was carried out using the HighScorePlus and FullProf software.

The method of iodometric titration was used to determine the average valence of iron ions in the air at room temperature for a model where the cation sublattice of bismuth ferrite doped by lanthanum can contain Bi^{3+}, La^{3+}, Fe^{2+}, Fe^{3+}, Fe^{4+} ions. In this case, the principle of electrical neutrality can be achieved as a result of both changes in a valence of iron and an oxygen index with the appearance of anion vacancies. The method of iodometric titration allows to determine the oxygen index in $ABO_{3-\delta}$ perovskites, which contain variable valence 3*d*-ions in *B*-positions, with an accuracy of $\delta = \pm 0.02$ per formula unit [41]. Such a systematic error in the determination of the oxygen content and the corresponding 0.02/3 relative error allow to calculate the filling factors for the *A*- and *B*-positions in a real $ABO_{3-\delta}$ perovskite structure with an accuracy up to 1%.

The non-stoichiometry, defect chemistry of a vacancy type and oxygen content were determined on the basis of comparative analysis of the X-ray diffraction, thermogravimetric and iodometric titration experimental data as well as previously established defect formation mechanism for ABO_3 perovskites [42–44]. Refinement of the oxygen index and verification of the correctness of the molar formulas obtained for the real $BiFeO_{3-\delta}$ and $Bi_{0.9}La_{0.1}FeO_{3-\delta}$ structures were controlled by the established early correlation between the relative change of the lattice parameter $\Delta a/a$ and the relative change of the average ionic radius $\Delta\bar{R} / \bar{R}$ in a perovskite structure [42].

The microstructure and size of crystallites in the ceramic samples were determined by the scanning electron microscopy (SEM) method using JEOL JSM-6490LV and FEI Magellan 400 scanning microscopes. The elemental analysis was carried out by the energy dispersive X-ray spectroscopy method. The survey was carried out in the mode of secondary and back scattered electrons with an

accelerating voltage of 20 kV with a magnification of 30–20000 times and focusing the electron beam on the sample surface up to 10 nm.

X-ray photoelectron spectra of the ceramics and initial Fe_2O_3, Bi_2O_3, La_2O_3 oxide powders were obtained at room temperature with the X-ray photoelectron microprobe ESCALAB 250. The spectra were excited with a monochromatized radiation of AlK_α. Clean surfaces of the samples were obtained by a diamond scribing file in a vacuum chamber under pressure of about 10^{-6} Pa. The state of the surfaces was monitored with C1s line with a very small intensity. However, the line was still detectable on the background which allowed using it for the calibration of the energy scales for all spectra. C1s line binding energy was taken to be 285 eV. The flow of slow electrons was used to counteract the charging of samples. The absolute energy resolution was 0.6 eV that was determined from the $Ag3d_{5/2}$ line profile. The Fe_2O_3, Bi_2O_3 and La_2O_3 powders were deposited by fine layer on a double-sided conductive adhesive tape. The flow of slow electrons was used to counteract the charging of powders as well. The background of X-ray photoelectron lines was cut off by Shirley [45].

The dielectric properties were studied on the basis of the analysis of the frequency dependences of the relative dielectric constant, $\varepsilon'(f)$, and the dielectric loss tangent, $\tan\Delta(f)$, measured by the dielectric spectroscopy in the LF (f = 1 Hz – 1 MHz) and UHF (f = 8.24–12.05 GHz) ranges at room temperature [46,47].

Magnetic measurements were carried out by using Quatum Design SQUID MPMS 3. Magnetic properties were determined on the basis of the analysis of the temperature $M(T)$ and magnetic field $M(H)$ dependences of magnetization. The $M(T)$ dependences were measured in two $M_{ZFC}(T)$ and $M_{FC}(T)$ modes, when the sample was heated after its cooling in a zero magnetic field (ZFC–mode) and when the sample was cooled in a magnetic field (FC–mode). The $M_{ZFC}(T)$ and $M_{FC}(T)$ dependences were measured in two magnetic fields of H = 50 Oe and 7 T. The hysteresis $M(H)$ curves were measured in a magnetic field up to 7 T at T = 4 and 300 K.

3. Structure and microstructure

An analysis of the X-ray patterns for the ceramic $BiFeO_3$ and $Bi_{0.9}La_{0.1}FeO_3$ samples obtained under different pressures P = 200 and 400 MPa (see Fig. 1) allows to conclude that the matrix structure of all samples studied is a rhombohedrally distorted hexagonal perovskite structure. In the $BiFeO_3$ sample (P = 200 MPa), a rhombohedral $R3m$ type of distortion with the lattice parameters of a = 5.5737 Å and c = 6.9339 Å and the unit cell of Z = 3 formula units is observed. In this sample, the available of additional phases of the $Bi_2Fe_4O_9$ with a mullite structure (orthorhombic $Pbam$ structure; a = 7.965 Å, b = 8.44 Å, c = 5.994 Å; Z = 2; ICCD No. 55) and $Bi_{25}FeO_{40}$ with a sillenite structure (cubic $I23$ structure; a = 10.1812 Å; Z = 1; ICCD No. 197) was observed as well. The content of each phase does not exceed 2 vol. %. The diffraction maxima for the $Bi_2Fe_4O_9$ and $Bi_{25}FeO_{40}$ are indicated by the * symbol in the region of angles 2θ = 27.5–29.0° (see Fig. 1 (*a*)). With increase in the pressure up to P = 400 MPa, the lattice parameters decrease and the structure is a rhombohedrally $R\bar{3}m$ distorted with a = 5.5694 Å and c = 6.8927 Å parameters. In this sample, the content of the perovskite phase decreases to 79.5 % and instead of the $Bi_2Fe_4O_9$ and $Bi_{25}FeO_{40}$ the phases of Bi_2O_3 oxide (cubic $I23$ structure, a = 10.08 Å, Z = 12, ICCD No. 197) and metallic Bi_4 bismuth (monoclinic $C2/m$ structure, a = 6.67256 Å, b = 6.1108 Å, c = 3.30013 Å, Z = 1, ICCD No. 10) are appeared with concentrations of 12.6 and 7.9 %, respectively (see Table 1). The diffraction maxima of the Bi_2O_3 and Bi_4 phases in Fig. 1 (*b*) are within the region of 2θ = 28.0 – 29.3° angles.

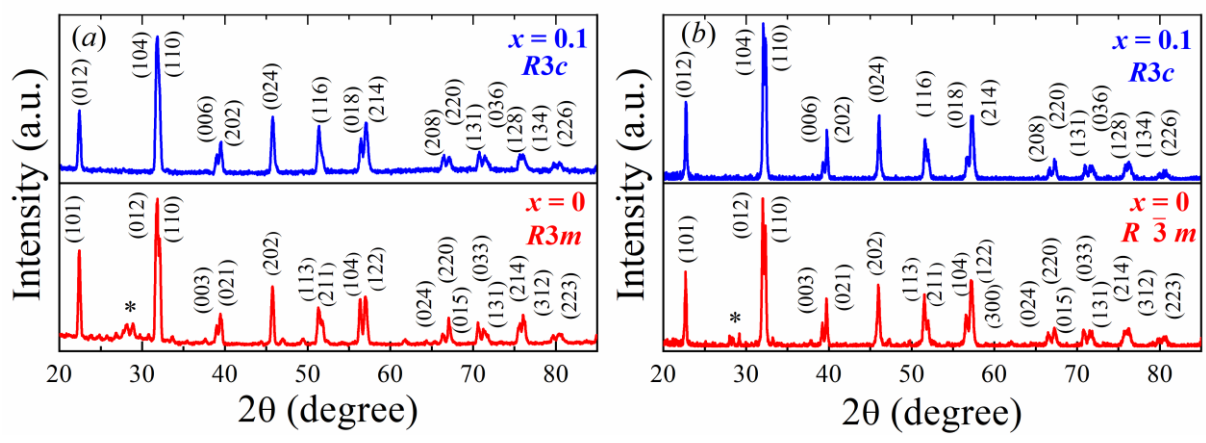

Fig. 1. X-ray patterns for the $Bi_{1-x}La_xFeO_3$ ceramics with x = 0 and 0.1 obtained by the RLS method under different pressures of P = 200 (*a*) and 400 MPa (*b*). The symbol * denotes the region of the diffraction maxima from the second additional phases.

While replacing bismuth with lanthanum, all $Bi_{0.9}La_{0.1}FeO_3$ samples, regardless of pressure *P*, are single-phase and have a rhombohedral *R*3*c* type of distortion (see Fig. 1). The lattice parameters vary from *a* = 5.5730 Å and *c* = 13.8480 Å for a sample with *P* = 200 MPa to *a* = 5.5734 Å and *c* = 13.8025 Å for a sample with *P* = 400 MPa (see Table 1). An absence of diffraction maxima in the region of 2θ = 27.5–29.3° angles indicates the complete polymorphic transformation of the initial oxides to the $Bi_{0.9}La_{0.1}FeO_3$ perovskite without the formation of the additional $Bi_2Fe_4O_9$, $Bi_{25}FeO_{40}$, Bi_2O_3 and Bi_4 phases.

At analyzing the X-ray data, two facts should be noted.

Firstly, in the $BiFeO_3$ sample, the *R*3*m* (*P* = 200 MPa) and $R\bar{3}m$ (*P* = 400 MPa) types of rhombohedral distortion are found (see Table 1), but the *R*3*c* type of distortion was observed for the hexagonal $BiFeO_3$ multiferroic [10]. The appearance of the *R*3*m* phase is possible at high temperatures when the cubic $Pm\bar{3}m$ structure of the perovskite is transformed to the *R*3*c* structure through two intermediate $R\bar{3}c$ and *R*3*m* phases [48,49]. The nonpolar $R\bar{3}c$ phase appears when the structure is distorted by only the rotation of the FeO_6 octahedra around the [111] axis without displacing the ions along the [111] direction [50]. The ferroelectric *R*3*m* phase appears with polar distortions, which is caused by the displacement of ions along [111] direction without rotation of the FeO_6 octahedra [48]. Interpreting the result, it can be said that the rapid cooling of the samples using the RLS method freezes the structure in an intermediate state at which the displacement of ions along [111] axis has already begun, but the rotation of the FeO_6 octahedra has not occurred. It should be noted that the *R*3*m* distortion of the structure prevents the appearance of the linear ME effect [51].

Secondly, the results of the phase analysis indicate the appearance of the Bi_2O_3 bismuth oxide and metallic Bi_4 bismuth in the $BiFeO_3$ (*P* = 400 MPa) sample instead of the phases of the $Bi_2Fe_4O_9$ mullite and $Bi_{25}FeO_{40}$ sillenite. It should be noted that with the appearance of the Bi_4 a sharp decrease in the lattice parameter *a* from 5.5737 to 5.5694 Å is observed with an increase in the pressure *P* from 200 to 400 MPa (see Table 1). Such a decrease in *a* parameter is possible as a result of the chemical pressure

because of the influence of metallic bismuth being in the intercrystalline zones of the $BiFeO_3$ microstructure.

Table 1

Phase composition, type of structure and lattice parameters for the $BiFeO_3$ and $Bi_{0.9}La_{0.1}FeO_3$ obtained by the RLS method under different pressures of P = 200 and 400 MPa

x	P (MPa)	Space group	ICDD No.	Lattice parameters			Second phase, vol.%			
				hexagonal		primitive				
				a (Å)	c (Å)	a_P (Å)	$Bi_{25}FeO_{40}$	$Bi_2Fe_4O_9$	Bi_2O_3	Bi_{14}
0	200	$R3m$	160	5.5737	6.9339	3.9620	< 2	< 2	–	–
0.1	200	$R3c$	161	5.5730	13.8480	3.9597	–	–	–	–
0	400	$R\bar{3}m$	166	5.5694	6.8927	3.9520	–	–	12.6	7.9
0.1	400	$R3c$	161	5.5734	13.8025	3.9555	–	–	–	–

The results of the SEM investigations for the microstructure of the $BiFeO_3$ and $Bi_{0.9}La_{0.1}FeO_3$ samples are shown in Fig. 2. The SEM spectroscopy data confirmed the chemical and phase composition for all samples. The $Bi_2Fe_4O_9$ impurity is located in an intergranular space of the $BiFeO_3$ (P = 200 MPa) and denotes as white spots in Fig. 2 (*a*). Assumption about the localization of the metallic Bi_4 bismuth in the crystallite boundaries of the $BiFeO_3$ (P = 400 MPa) is confirmed by Fig. 2 (*f*).

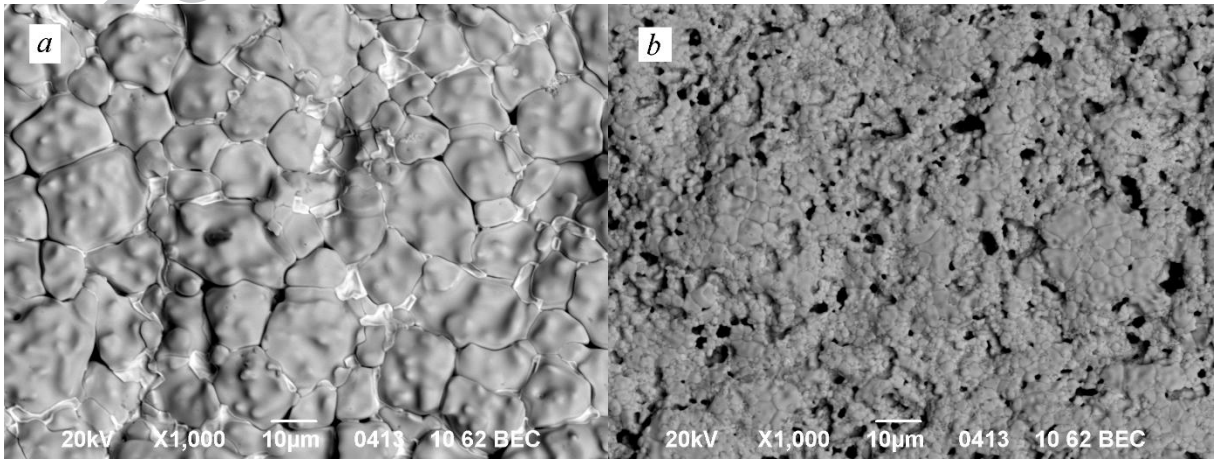

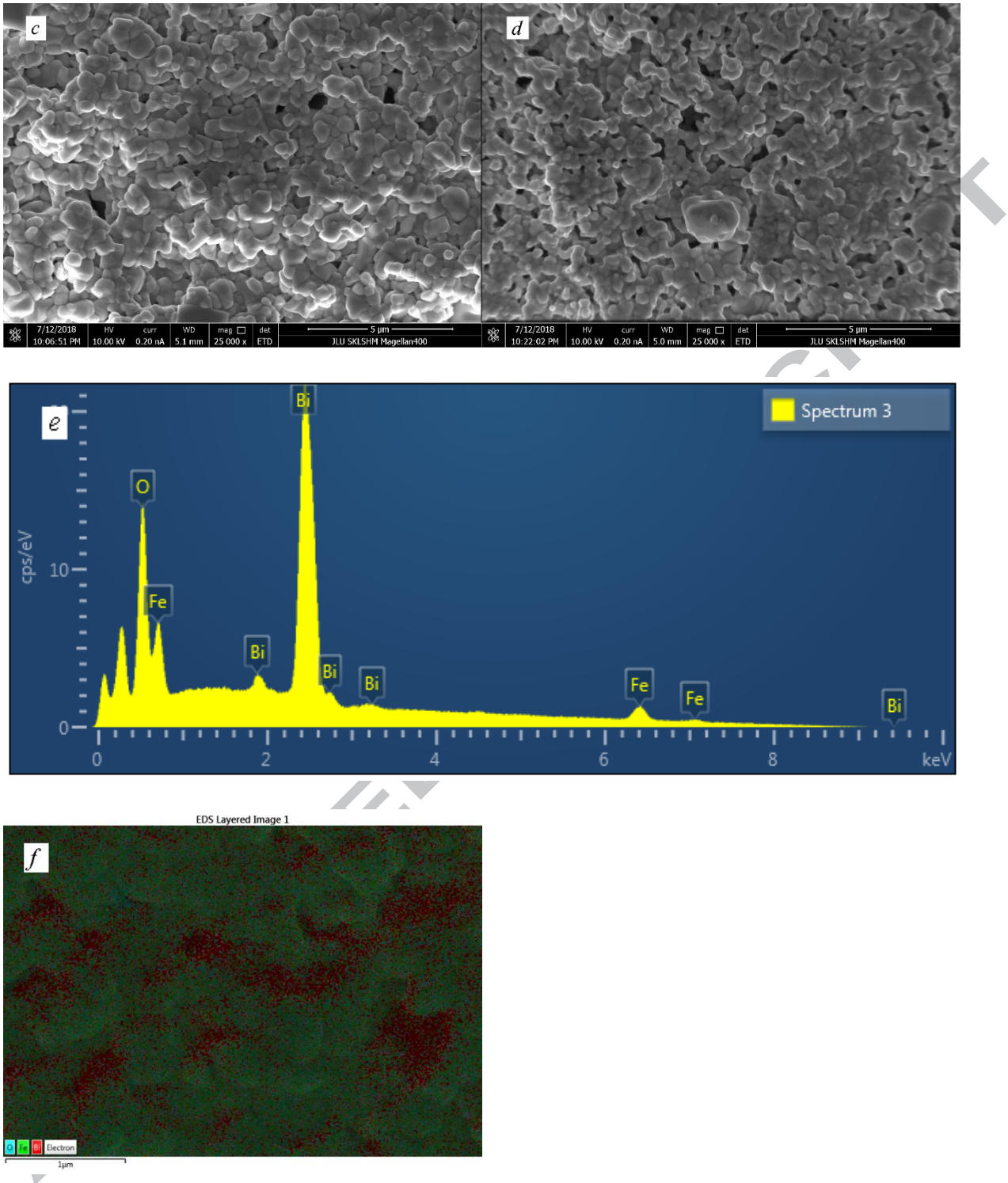

Fig. 2. Microstructure of the $BiFeO_3$ (*a*) and $Bi_{0.9}La_{0.1}FeO_3$ (*b*) under *P* = 200 MPa, the $BiFeO_3$ (*c*) and $Bi_{0.9}La_{0.1}FeO_3$ (*d*) under *P* = 400 MPa as well as EDS pattern of the $BiFeO_3$ (*e*) under *P* = 400 MPa and increased concentration of bismuth in the vicinity of crystallite boundaries for the $BiFeO_3$ (*f*) under *P* = 400 MPa obtained by the SEM method.

According to the SEM investigations, the crystallite size decreases from ~ 10 to ~ 1 μm (see Fig. 2 (*a*) and (*b*)) for the samples obtained at *P* = 200 MPa when bismuth is replaced by lanthanum. It leads to the formation of finely porous cellular microstructure in the $Bi_{0.9}La_{0.1}FeO_3$. Such type of the

microstructure should accumulate a large charge in the LF range. With increasing the pressure *P* from 200 to 400 MPa, the microstructure of the samples shows a well-formed surface consisting of small crystallites, the average size of which slightly varies from ~ 500 nm in the $BiFeO_3$ (*P* = 400 MPa) to ~ 450 nm in the $Bi_{0.9}La_{0.1}FeO_3$ (*P* = 400 MPa) with increasing La content.

4. Non-stoichiometry and molar formulas of a real structure

In bismuth ferrite, an isovalent substitution of Bi^{3+} for La^{3+} ions with the same ionic radii should not result in the significant changes in its structural properties, since with such a substitution neither changes in the valence of other ions, nor changes in interionic distances should occur [52]. To explain such changes, it is necessary to introduce an additional parameter into consideration. This parameter is a non-stoichiometry. The non-stoichiometry depends on the concentration of the cation $V^{(c)}$ and anion $V^{(a)}$ vacancies and affects the valence and charge state of cations, the length of metal-oxygen bonds, the coordination number and heterogeneity of the coordination environment, which leads to the changes in the stability of structure and its properties.

The appearance of the $V^{(c)}$ and $V^{(a)}$ vacancies in the perovskite structure is observed at high temperatures of synthesis and annealing. The $V^{(a)}$ vacancies are formed as a result of the thermal dissociation in the positions formally occupied by oxygen vented to the atmosphere. Reduction of an iron to Fe^{2+} preserves the electroneutrality of a unit cell. The appearance of $V^{(c)}$ occurs during the oxidative process while the sample is cooled after the appearance of new metal-oxygen bonds at the "solid solution-atmosphere" interface. As a result of the greater mobility of a cation sublattice [43], the $V^{(c)}$ vacancies are formed at the site of the cations moved to the interface.

On the basis of the defect formation mechanism taking into account the phase composition [53], X-ray diffraction and thermogravimetric data as well as the results of iodometric titration for determining the average iron valence [42], the molar formulas of the real $BiFeO_{3-\delta}$ and $Bi_{0.9}La_{0.1}FeO_{3-\delta}$ structure were determined (see Table 2). The molar formulas were determined taking into account the fact that the Bi^{3+}, Bi^{5+}, Fe^{3+}, Fe^{2+}, O^{2-} ions as well as the $V^{(c)}$ and $V^{(a)}$ vacancies can be in the perovskite structure.

Table 2

The molar formulas of the real perovskite structure and concentration of the anion $V^{(a)}$ vacancies for the $BiFeO_{3-\delta}$ and $Bi_{0.9}La_{0.1}FeO_{3-\delta}$ ceramics obtained under different pressure *P*

x	*P* (MPa)	Molar formulas of defect perovskite structure	$V^{(a)}$ (%)
0	200	$\{Bi^{3+}_{0.99}V^{(c)}_{0.01}\}_A[Fe^{2+}_{0.38}Fe^{3+}_{0.61}V^{(c)}_{0.01}]O^{2-}_{2.78}V^{(a)}_{0.22}$	7.3
0.1	200	$\{Bi^{3+}_{0.88}La^{3+}_{0.10}V^{(c)}_{0.02}\}_A[Fe^{2+}_{0.27}Fe^{3+}_{0.72}V^{(c)}_{0.01}]_BO^{2-}_{2.82}V^{(a)}_{0.18}$	6.0
0	400	$\{Bi^{3+}_{0.99}V^{(c)}_{0.01}\}_A[Fe^{2+}_{0.10}Fe^{3+}_{0.89}V^{(c)}_{0.01}]O^{2-}_{2.92}V^{(a)}_{0.08}$	2.7
0.1	400	$\{Bi^{3+}_{0.88}La^{3+}_{0.10}V^{(c)}_{0.02}\}_A[Fe^{2+}_{0.05}Fe^{3+}_{0.94}V^{(c)}_{0.01}]_BO^{2-}_{2.93}V^{(a)}_{0.07}$	2.3

The real structure of the $BiFeO_{3-\delta}$ and $Bi_{0.9}La_{0.1}FeO_{3-\delta}$ is non-stoichiometric and in addition to the *A*-cations of Bi^{3+}, the *B*-cations of Fe^{3+} and Fe^{2+}, and the anions of O^{2-} oxygen it also contains the $V^{(a)}$ and $V^{(c)}$ vacancies (see Table 2). The quantity of the $V^{(c)}$ vacancies in the *A*- and *B*-positions is an insignificant to 1-2 % and it can be considered that the both cation sublattices are completely filled. The criterion for the correctness of definition of the molar formulas is the established correlation between the experimental values of the relative changes in the $\Delta a_P/a_P$ lattice parameter (a_P is a parameter of the primitive cell) and the calculated values of the relative changes in the $\Delta\bar{R}/\bar{R}$ average ionic radius [43,54]. To determine the relative changes $\Delta a_P/a_P$, the parameters of *a* and *c* of the hexagonal structure were recalculated for the a_R and α_R parameters of the rhombohedral structure [55]. Since the angle of the rhombohedral distortion α_R = 89.4 – 89.6° is slightly different from 90°, the parameter a_R can be considered as the parameter a_P of the primitive elementary cell for the studied samples (see Table 1 and Fig. 3).

The average ionic $\bar{R}$ radius was calculated from the equations [42], in which the fill factors of all crystallographic positions (see Table 2) and the radii of ions in according to their valence state and coordination number were used [52]. It should be noted that in an ideal cubic perovskite structure, a bismuth is in the *A*-position with CN = 12. In the rhombohedral *R*3*c* structure, the *A*-position is strongly

distorted and only 6 out of 12 oxygen anions are the nearest environment of bismuth [50], and thus, La and Bi in the *A*-positions are in the octahedra of LaO_6 and BiO_6 with CN = 6.

The correlation established between the relative changes of the $\Delta a_P/a_P$ parameter of the primitive cell and the average $\Delta\bar{R}/\bar{R}$ ionic radius of the perovskite structure for the $BiFeO_{3-\delta}$ and $Bi_{0.9}La_{0.1}FeO_{3-\delta}$ samples (see Fig. 3) confirms the correctness of the molar formulas of the real structure determined (see Table 2).

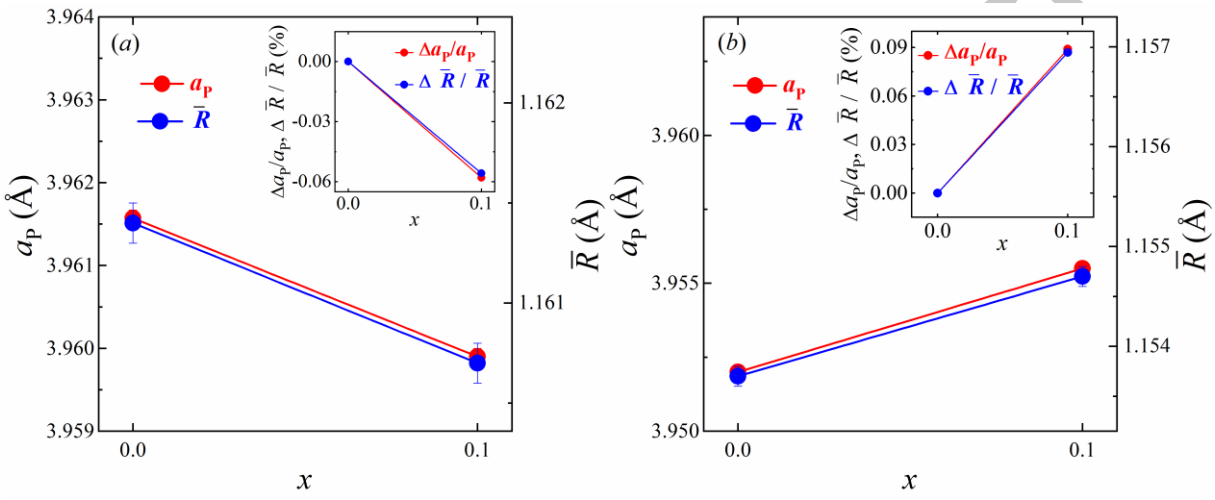

Fig. 3. Concentration changes in the parameter a_P of the primitive cell and the average $\bar{R}$ ionic radius for the perovskite $Bi_{1-x}La_xFeO_{3-\delta}$ structure under different pressures *P* = 200 (*a*) and 400 MPa (*b*). The inset shows the correlation between the relative changes in the $\Delta a_P/a_P$ parameter and the average $\Delta\bar{R}/\bar{R}$ ionic radius.

As can be seen from Table 2, all samples are non-stoichiometric in oxygen. With an increase in the La content, the concentration of the $V^{(a)}$ vacancies slightly decreases from 7.3 % in the $BiFeO_{3-\delta}$ to 6.0 % in the $Bi_{0.9}La_{0.1}FeO_{3-\delta}$ for *P* = 200 MPa and from 2.7 % in the $BiFeO_{3-\delta}$ to 2.3 % in the $Bi_{0.9}La_{0.1}FeO_{3-\delta}$ for *P* = 400 MPa. Increasing the pressure *P* from 200 to 400 MPa reduces the concentration of the $V^{(a)}$ vacancies in all compositions by almost 2.5 times. The deviation from stoichiometry ~ 1 % of the $V^{(c)}$ vacancies in the cation *A*- and *B*-sublattices is insignificant and does not depend either on the lanthanum content or the pressure *P*. The large concentration of Fe^{2+} in the *B*-positions is of particular interest. The amount of Fe^{2+} depends on the concentration of the $V^{(a)}$ vacancies, since a decrease in the oxygen sublattice of charge by anion vacancies at high synthesis temperatures is compensated by the appearance of Fe^{2+} in the cation sublattice. The high concentration of the $V^{(a)}$ and Fe_B^{2+} is the result of a rapid cooling

of the samples (100 °C/sec). At this cooling rate, the partially deoxidized Fe^{2+} cations have no time to reach the sample surface in order to oxidize to Fe^{3+}. This is the reason for the small deviation from stoichiometry in the cation sublattice and the high concentration of the $V^{(a)}$ and Fe_B^{2+} in the $BiFeO_{3-\delta}$ and $Bi_{0.9}La_{0.1}FeO_{3-\delta}$ samples under P = 200 MPa. As can be seen from Table 2, an increase in the pressure P from 200 to 400 MPa greatly reduces the concentration of Fe_B^{2+} from 38 to 10 % in the $BiFeO_{3-\delta}$ and from 27 to 5 % in the $Bi_{0.9}La_{0.1}FeO_{3-\delta}$. Such a significant effect of non-stoichiometry on the change in the valence state of iron ions in the bismuth ferrite should strongly influence its structure, magnetic and dielectric properties.

5. Structure, dielectric and magnetic properties of the non-stoichiometric single-phase $Bi_{0.9}La_{0.1}FeO_{3-\delta}$ composition

5.1. Structural properties of the non-stoichiometric $Bi_{0.9}La_{0.1}FeO_{3-\delta}$ perovskite

Since the greatest deviation from stoichiometry among single-phase samples is observed in the $Bi_{0.9}La_{0.1}FeO_{3-\delta}$ sample under P = 200 MPa with a concentration of $V^{(a)}$ = 7.3 % vacancies (see Table 2), the studying its structural properties in a wide temperature range is an increased interest.

According to X-ray diffraction data, the $Bi_{0.9}La_{0.1}FeO_{3-\delta}$ sample is a single-phase and has a rhombohedral *R*3*c* (ICDD: 98-001-5299) structure which is not changed within a temperature range from 18 to 290 K as shown in Fig. 4 and 5. An analysis of its crystal structure is performed in according to the model proposed [56]. The hexagonal unit cell of the $Bi_{0.9}La_{0.1}FeO_3$ composition contains six formula units (Z = 6) (Fig. 6). The lattice parameters of the solid $Bi_{0.9}La_{0.1}FeO_{3-\delta}$ solution monotonically decrease with a decrease of temperature (Fig. 7 and Table 3).

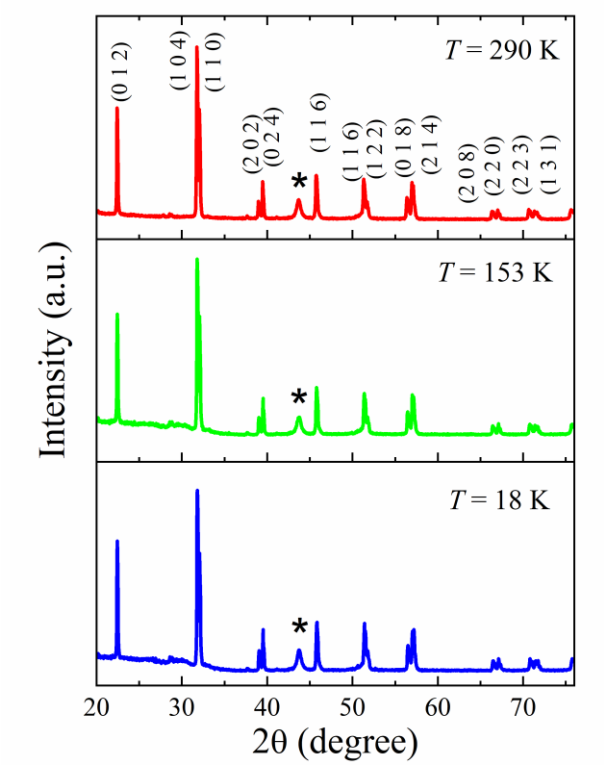

Fig. 4. X-ray patterns of the $Bi_{0.9}La_{0.1}FeO_{3-\delta}$ sample at different temperatures *T*. The label * denotes the reflex of the sample holder.

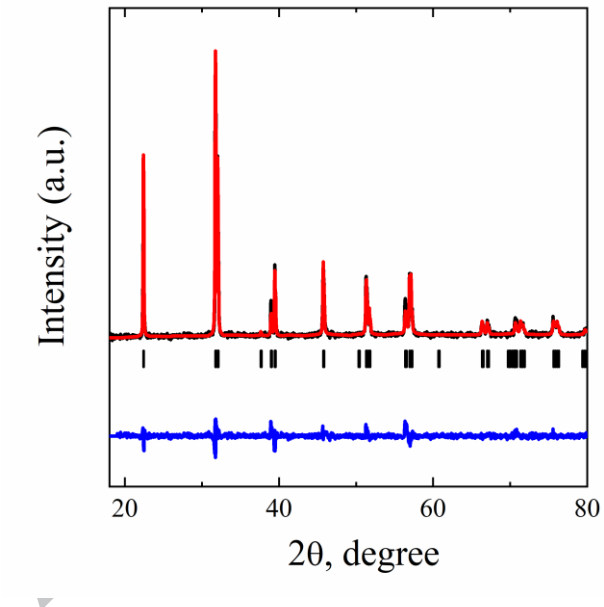

Fig. 5. X-ray pattern of the $Bi_{0.9}La_{0.1}FeO_{3-\delta}$ at room temperature treated by the Rietveld method. The experimental points, calculated function and difference curve normalized to the statistical error are shown. Vertical strokes designate the positions of the peaks for the $Bi_{0.9}La_{0.1}FeO_3$ crystal structure.

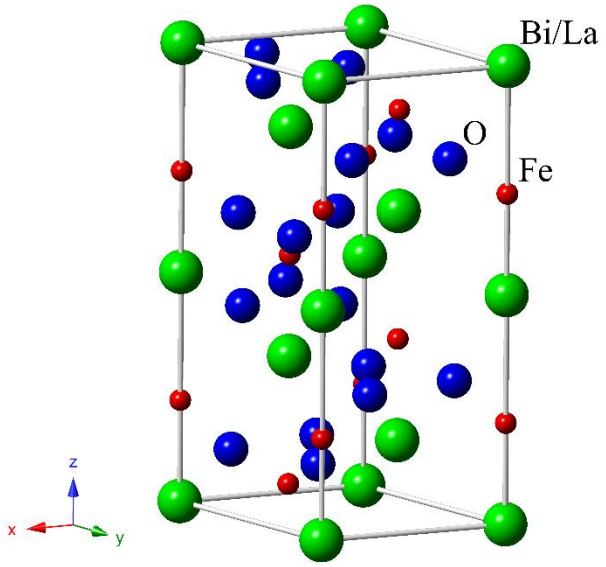

Fig. 6. The elementary cell for the $Bi_{0.9}La_{0.1}FeO_{3-\delta}$ in a hexagonal installation ploted by using data of Table 3. Ion indication: O is a blue color, Bi / La is a green color, Fe is a red color.

Table 3

The parameters of the $Bi_{0.9}La_{0.1}FeO_{3-\delta}$ crystal structure, standard calculation and experimental factors, coordinates of the atoms determined by the Rietveld method within the framework of the space group *R*3*c* (№ 161) at different temperatures. The ions are in the positions of Bi/La (6a) (0, 0, 0); Fe (6a) (0, 0, *z*); O (18b) (*x*, *y*, *z*)

T	Structure parameters and criteria of fit										
(K)	*a* (Å)	*c* (Å)	*V* (Å^3)	Fe (6a)	O (18b)			R_{exp}	R_p	R_{wp}	χ^2
				z	*x*	*y*	*z*	(%)	(%)	(%)	
18	5.5695(2)	13.8139(5)	371.09(2)	0.216(1)	1.023(8)	0.585(9)	0.966(3)	21.95	44.2	24.9	1.28
30	5.5691(1)	13.8127(4)	371.00(2)	0.217(1)	1.013(7)	0.572(9)	0.962(3)	21.95	43.8	24.6	1.26
60	5.5696(1)	13.8155(5)	371.15(2)	0.217(1)	1.023(7)	0.575(9)	0.964(3)	21.95	43.1	24.4	1.23
90	5.5703(1)	13.8179(5)	371.30(2)	0.217(1)	1.025(7)	0.579(9)	0.962(3)	22.10	43.9	24.5	1.23
120	5.5708(2)	13.8204(4)	371.44(1)	0.217(1)	1.020(7)	0.578(9)	0.964(3)	22.25	43.0	23.9	1.16
190	5.5730(2)	13.8293(4)	371.97(2)	0.217(1)	1.025(7)	0.579(9)	0.961(3)	22.26	44.3	24.3	1.19
230	5.5744(2)	13.8346(5)	372.30(2)	0.217(1)	1.026(7)	0.585(8)	0.963(3)	22.44	43.9	24.1	1.16
290	5.5778(1)	13.8492(4)	373.15(1)	0.220(7)	0.997(6)	0.566(8)	0.963(2)	18.62	37.7	22.9	1.51

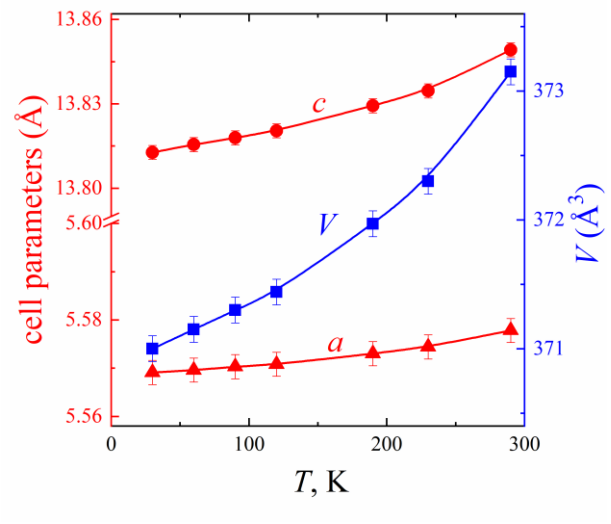

Fig. 7. Temperature dependences of the lattice parameters, *a* and *c*, and the volume cell, *V*, for the $Bi_{0.9}La_{0.1}FeO_{3-\delta}$.

On the basis of the analysis of X-ray diffraction data, the microstructural parameters of the $Bi_{0.9}La_{0.1}FeO_3$ ceramics were additionally determined. The microstrain ε and an average size of the coherent scattering region $<D_{CSR}>$ were equal to 0.16 % and 820 nm, respectively. This size is close to the average crystallite size ~ 1 μm from SEM measurements (see Fig. 3(*b*)). The contributions of the real physical broadening were determined from the difference between a broadening of the diffraction peaks of the $Bi_{0.9}La_{0.1}FeO_3$ and calibration LaB_6 samples. The separation of the ε and $<D_{CSR}>$ contributions into the broadening of the observed diffraction peaks was performed by the Williamson-Hall method [57]. Using the HighScorePlus software, the Debye-Scherrer method additionally allowed to determine ε = 0.179 % and $<D_{CSR}>$ = 137.3 nm. The discrepancies obtained by two methods in the sizes of the coherent scattering region are observed. In the Debye-Scherrer method, a single diffraction line located in a region of small angles θ is used. In the Williamson-Hall method, an analysis is conducted for all lines with extrapolation to the region of small angles excluding the contribution from microstrains.

5.2. Valence states in the single-phase non-stoichiometric $Bi_{0.9}La_{0.1}FeO_{3-\delta}$ perovskite

Fig. 8 shows a comparative analysis of the X-ray photoelectron spectra of the initial Fe_2O_3 powder and the $Bi_{0.9}La_{0.1}FeO_{3-\delta}$ (*P* = 200 MPa) sample. As shown in Fig. 8 and Table 4, Fe2p spectrum of the Fe_2O_3 powder consists of two maxima A and C at a distance of 13.6 eV related to $Fe2p_{3/2}$ and $Fe2p_{1/2}$

levels, respectively. In addition to these main features of the spectra, at a distance of 7.8 eV from the maximum of A there is a singularity B (719 eV) and after the peak C there is a diffuse shelf D (733 eV). The features of C and D refer to satellites of charge transfer. Moreover, the availability of singularity C and the value of binding energy equal to 711.2 eV indicate that the iron ions in the investigated powder are in the trivalent state [58,59].

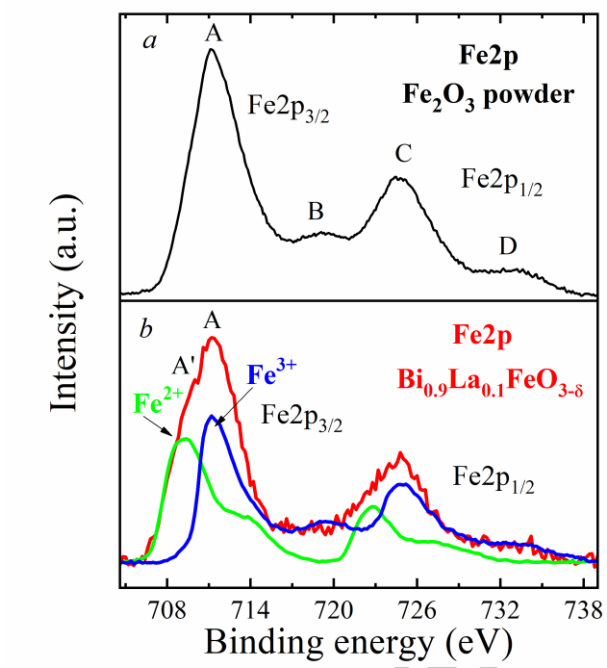

Fig. 8. X-ray photoelectron spectra of Fe2p for the Fe_2O_3 powder (*a*) and the $Bi_{0.9}La_{0.1}FeO_{3-\delta}$ (*P* = 200 MPa) sample (*b*) and its decomposition into components related to the Fe2p spectrum from Fe^{2+} ions (green curve) and Fe^{3+} (blue curve).

Fig. 8 (*b*) shows the appearance of an additional bend A' in the spectrum for the $Bi_{0.9}La_{0.1}FeO_{3-\delta}$ sample. This bend A' has energy lower than the maximum of A at a distance of about 1.8 eV. In addition, there is no feature B in the spectrum. These differences from Fe2p spectrum in Fig. 8 (*a*) allow to conclude that the spectrum for the Fe_3O_4 sample [59], which has Fe^{2+} and Fe^{3+} ions, is the similar to Fig. 8 (*b*).

Table 4

The binding energies of Fe2p, Bi4f, La3d, and O1s levels in the $Bi_{0.9}La_{0.1}FeO_{3-\delta}$ ceramics and the Fe_2O_3, Bi_2O_3, La_2O_3 powders

Sample	Binding energies of levels						
	Fe2p		Bi4f		La3d		O1s
	$2p_{3/2}$	$2p_{1/2}$	$4f_{7/2}$	$4f_{5/2}$	$3d_{5/2}$	$3d_{1/2}$	
Fe_2O_3	711.2	724.8	–	–	–	–	530.3
Bi_2O_3	–	–	158.7	164.0	–	–	530.0
La_2O_3	–	–	–	–	834.5	851.1	530.9
$Bi_{0.9}La_{0.1}FeO_{3-\delta}$	711.3	724.8	158.7	164.0	834.4	850.8	529.9

To clarify the available of different valance iron ions in the ceramic $Bi_{0.9}La_{0.1}FeO_{3-\delta}$ sample the experimental spectrum was decomposed (see Fig. 8 (*b*)) using the approach described for the components related to bivalent and trivalent iron ions [58]. Fe2p spectra of divalent and trivalent iron used as components of decomposition were taken by analogy with work [58]. Fe2p spectrum of the ceramic sample is described quite well by the sum of the components related to Fe^{2+} and Fe^{3+} with proportions of 26 % and 74 %, respectively (see Fig. 8). At estimating the contributions, it was taken into account that the ionization probability of the 2p shell in Fe^{2+} ion is twice higher than in Fe^{3+} ion [58]. These values correspond to the values of 27.3 % (Fe^{2+}) and 72.7 % (Fe^{3+}) obtained from the molar formulas of the real structure with very good accuracy (see Table 2). Therefore, the availability of different valence iron Fe^{2+} and Fe^{3+} ions in the $Bi_{0.9}La_{0.1}FeO_{3-\delta}$ sample at the isovalent substitution of Bi^{3+} by La^{3+} ions has been confirmed by XPS method as well.

The analysis of X-ray photoelectron spectra of Bi4f (see Fig. 9 (*a*)) shows that they practically coincide and have the same energies (Table 4). The spectra have two components, $Bi4f_{7/2}$ and $Bi4f_{5/2}$,

separated by a spin-orbital interaction. The energy position of $Bi4f_{7/2}$ component equals to 158.7 eV in both samples that suggests the trivalent state of bismuth in the $Bi_{0.9}La_{0.1}FeO_{3-\delta}$ [58].

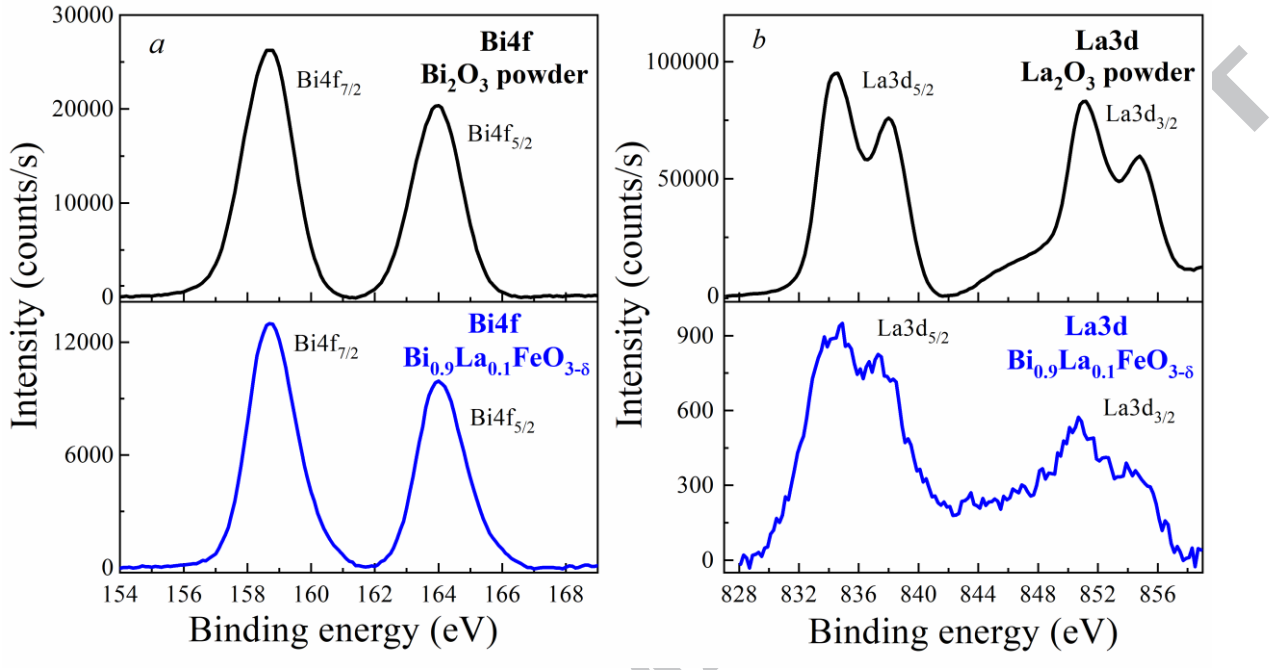

Fig. 9. X-ray photoelectron spectra of Bi4f for the Bi_2O_3 powder and the $Bi_{0.9}La_{0.1}FeO_{3-\delta}$ ceramics (*a*) and of La3d for the La_2O_3 powder and the $Bi_{0.9}La_{0.1}FeO_{3-\delta}$ ceramics (*b*).

Fig. 9 (*b*) shows X-ray photoelectron spectra of La3d. The nominal content of lanthanum in the $Bi_{0.9}La_{0.1}FeO_{3-\delta}$ sample is 1 mol. %. Despite the low content of lanthanum, we were able to obtain $La3d_{5/2}$ and $La3d_{3/2}$ spectra, although with much worse statistics. Nevertheless, the main contours of $La3d_{5/2}$ and $La3d_{3/2}$ are reproduced. In addition, it was possible to determine the energy of maximum component of $La3d_{5/2}$ and $La3d_{3/2}$ peaks (Table 4). As shown in Fig. 9 (*b*), the spectra are almost identical and have the same energy (Table 4). The La3d spectra were calculated [60]. In the one-electron approximation, the spectra have two components of $La3d_{5/2}$ and $La3d_{3/2}$ which are separated by the spin-orbital interaction. In addition to these main features of the spectra, they have an extra fine structure due to the availability of charge transfer satellites, plasmon satellites and contribution of the Auger-line MNN components [61]. A detailed analysis of La3d spectrum for the La_2O_3 was conducted [60–62]. According to these papers, sufficient broad features, located at 13.5 eV on the high-energy side of each main doublet line, is due to from Auger MNN electron lines and plasmon excitations. Expressed features on the main components, located approximately 4 eV from the main maximum of each line, are the charge transfer satellites

reflecting the formation of the screening states $3d^{-1}\ 4f^{1}L^{-1}$ (L = ligand), during "shaking off" the valence electrons on free 4f-orbitals [62]. The equal energy position of $La3d_{5/2}$ and $La3d_{3/2}$ components for the La_2O_3 powder and the $Bi_{0.9}La_{0.1}FeO_{3-\delta}$ ceramics allows to conclude that the lanthanum ions in the $Bi_{0.9}La_{0.1}FeO_{3-\delta}$ sample are in the trivalent state.

5.3. Dielectric properties of the single-phase $Bi_{0.9}La_{0.1}FeO_{3-\delta}$ multiferroics with varying non-stoichiometry δ

The investigation of dielectric properties for the $Bi_{0.9}La_{0.1}FeO_{3-\delta}$ multiferroics has showed that the complex relative dielectric permittivity $\varepsilon^{*} = \varepsilon' + i\varepsilon''$ and dielectric loss tangent $\tan\Delta = \varepsilon'' / \varepsilon'$ have a relaxation type of dispersion (Fig. 10). At room temperature, the $Bi_{0.9}La_{0.1}FeO_{3-\delta}$ (P = 200 MPa) with oxygen non-stoichiometry δ = 0.18 (see Table 2) has anomalously high values of the $\varepsilon' = 5\cdot10^{5}$ at 1 Hz, the values of which exponentially decrease to $\varepsilon' \sim 209$ with increase in a frequency to f = 1 MHz. In the $Bi_{0.9}La_{0.1}FeO_{3-\delta}$ (P = 400 MPa) with δ = 0.07, the dielectric permittivity decreases sharply to $\varepsilon' = 82$ at 1 Hz and then slightly decreases to $\varepsilon' = 50$ with increasing frequency to f = 1 MHz (see Fig. 10). The colossal values of the ε′ in the LF range for the $Bi_{0.9}La_{0.1}FeO_{3-\delta}$ (P = 200 MPa) sample, as we expect, are associated to the charge accumulation at the boundaries of the finely crystalline structure (see Fig. 2 (*b*)).

In the UHF range f = 8 – 12 GHz, the relative permittivity ε_∞ and dielectric loss tanΔ become frequency-independent for all samples. With decreasing non-stoichiometry δ from 0.18 to 0.07, a decrease in ε_∞ from 10.5 (P = 200 MPa) to 7.7 (P = 400 MPa) and an increase in tanΔ from $1.7\cdot10^{-3}$ (P = 200 MPa) to $1.3\cdot10^{-2}$ (P = 400 MPa) are observed. It should be noted that for the pure $BiFeO_{3-\delta}$ bismuth ferrite, the values of the ε_∞ and tanΔ are equal to 34.5 and $2.9\cdot10^{-3}$ for δ = 0.22 and equal to 13.6 and $3.9\cdot10^{-3}$ for δ = 0.08, respectively. Such high values of ε_∞ for the $BiFeO_{3-\delta}$ are possibly associated to the influence of the $Bi_2Fe_4O_9$ and $Bi_{25}FeO_{40}$ impurity phase (see Table 1).

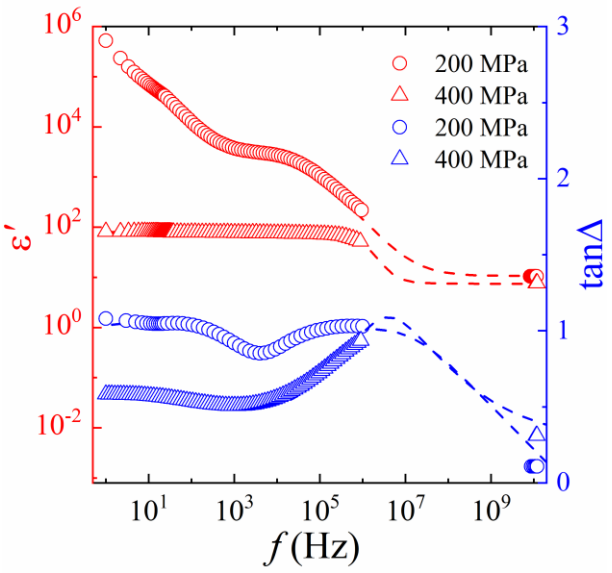

Fig. 10. Frequency dependences of the ε′(*f*) permittivity and the tanΔ(*f*) loss for the $Bi_{0.9}La_{0.1}FeO_{3-\delta}$ ceramics obtained under different pressures of *P* = 200 and 400 MPa. The fitting curves obtained from equations (1) and (2) are indicated by a dashed line.

The model spectra of the ε^* components, which are in good agreement with the experimental data, can be described by the relations [63–65]:

$$\varepsilon' = \varepsilon_\infty + \frac{(\varepsilon_s-\varepsilon_\infty)[1+(\omega\tau)^{1-\alpha}\sin(\pi\alpha/2)]}{1+2(\omega\tau)^{1-\alpha}\sin(\pi\alpha/2)+(\omega\tau)^{2(1-\alpha)}} + \frac{(\varepsilon_{s1}-\varepsilon_{\infty1})[1+(\omega\tau_2)^{\gamma}\sin(\pi\gamma/2)]}{1+2(\omega\tau_2)\sin(\pi\gamma/2)+(\omega\tau_2)^{2\gamma}} + \frac{\sigma_1}{\varepsilon_o\omega^{\beta_1}}, \quad (1)$$

$$\varepsilon'' = \frac{(\varepsilon_s-\varepsilon_\infty)(\omega\tau)^{1-\alpha}\cos(\pi\alpha/2)}{1+2(\omega\tau)^{1-\alpha}\sin(\pi\alpha/2)+(\omega\tau)^{2(1-\alpha)}} + \frac{(\varepsilon_{s1}-\varepsilon_{\infty1})(\omega\tau_2)^{\gamma}\cos(\pi\gamma/2)}{1+2(\omega\tau_2)\sin(\pi\gamma/2)+(\omega\tau_2)^{2\gamma}} + \frac{\sigma_2}{\varepsilon_o\omega^{\beta_2}}, \quad (2)$$

where ε_s is a static dielectric permittivity, ε_∞ is a high-frequency dielectric permittivity. The parameters α, γ, β characterize the distributions of the relaxation times τ determined in the first approximation from the condition $\omega_{max}\cdot\tau = 1$, where ω_{max} is a frequency corresponding to the maximum of tanΔ. The second and third terms in Eq. (1) are mathematical expressions describing the Debye model in different frequency intervals with the Cole-Cole and Cole-Davidson distributions of relaxation times [63,64], respectively.

The second term in Eq. (1) can be related to the electron hopping mechanism between $Fe^{2+} \leftrightarrow Fe^{3+}$ ions, which is in the frequency range from 10^3 to 10^6 Hz [66,67]. In this frequency range, the decrease observed in the tanΔ while decreasing non-stoichiometry δ well correlates with the decrease in the amount of Fe^{2+} ions (see Table 2 for *x* = 0.1). An insufficient frequency dependence of the real component of the dielectric constant for the sample synthesized under *P* = 400 MPa is due to the low

polarization of the highly localized states of Fe^{3+} ions. In the sample obtained under P = 200 MPa, the fraction of Fe^{2+} ions is significantly higher, that promotes an increase in dielectric losses in this frequency range.

The third term in Eq. (1) describes the high-frequency relaxation mechanism of the dielectric polarization, the nature of which has not been finally clarified. A possible mechanism of the dielectric polarization in the frequency range from 10^7 to 10^9 Hz is the motion of the walls of ferroelectric domains [67].

In the LF limit which is described by the last term in Eq. (1) and (2), the large values of the tanΔ are due to the contributions of quasi-free carriers of the electric current to the dielectric polarization, i.e. dielectric losses are related to the conductivity and accumulation of electric charge on the intercrystalline boundaries, inhomogeneities and structure defects within a framework of the Maxwell-Wagner and Kups models [25,68]. The using of Eq. (1) and (2) allows to obtain model spectra (see Fig. 10). The deviation between the theoretical calculations and the experimental data does not exceed an error of the experiment within the frequency interval. The parameters of the model spectra are given in Table 5.

Table 5

The dielectric τ, α, ε_s, ε_∞, σ_1, β_1, σ_2, β_2, τ_2, γ, ε_{s1}, $\varepsilon_{\infty 1}$ parameters of model spectra for the $Bi_{0.9}La_{0.1}FeO_{3-\delta}$ ceramics obtained by the RLS method under different pressure P

P (MPa)	τ (10^{-5} s)	α	ε_s	ε_∞	σ_1 ($10^{-7}\Omega^{-1}\cdot m^{-1}$)	β_1	σ_2 ($10^{-7}\Omega^{-1}\cdot m^{-1}$)	β_2	τ_2 (s)	γ	ε_{s1}	$\varepsilon_{\infty 1}$
200	3.92	0.05	2100	10.65	29.99	0.898	32.99	0.770	$1.26\cdot10^{-5}$	0.987	3700	2100
400	0.08	0.01	73	7.4	0.0001	0.500	0.0001	0.500	0.08	0.220	80	73

The increase in the value of real component of dielectric constant in the $Bi_{0.9}La_{0.1}FeO_{3-\delta}$ samples (P = 200 MPa) compared with the results obtained on the samples (P = 400 MPa) within the frequency range of $10^5 - 10^8$ Hz is associated to a large concentration of structure defects. The effect of structure

defects in Fig. 10 is shown in the region of notable relaxation behavior of dielectric functions. An increased content of anion vacancies (a large δ value) and a high content of Fe^{2+} (see Table 2) lead to a significant increase of the dielectric constant in the static limit. At a frequency $f \rightarrow 0$, the formation of dielectric properties is influenced by the high conductivity of the samples due to the contribution to polarization. This contribution is caused by the availability of quasi-free charge carriers which move within the crystallites under the action of an external alternating electric field. Charge accumulation at the crystallite boundaries provides the formation of a polarized state. This interpretation of the experimental data is supported by a large scatter of the relaxation times described by α and γ parameters as well as high conductivities σ_1 and σ_2 in the $Bi_{0.9}La_{0.1}FeO_{3-\delta}$ samples with P = 200 MPa (see Table 5). The availability of a minimum in the $\tan\Delta(f)$ dependence within the range $10^3 – 10^4$ Hz is due to the coexistence of different dielectric polarization mechanisms. With decreasing frequency, the processes associated with electron hopping between different valence cations of iron reach saturation, which leads to the establishment of a constant value of tanΔ. However, at a frequency corresponding to the minimum value of tanΔ, not all possible defects contribute to the polarization of the material. As the frequency decreases, the number of quasi-free charge carriers reacting to a change in the sign of the external electric field increases, which leads to an increase in the dielectric loss tangent. In the $Bi_{0.9}La_{0.1}FeO_{3-\delta}$ samples (P = 400 MPa), this mechanism does not affect the dielectric constant due to the small amount of Fe^{2+} ions that is evidenced by decreasing the α parameter in five times. A small value of the relaxation time τ corresponds to relatively high frequency, below which saturation occurs due to the contribution caused by electron hopping between different valence cations of iron. The availability of the last ones, though in a small amount (see Table 2), was found in the $Bi_{0.9}La_{0.1}FeO_{3-\delta}$ (P = 400 MPa). On the basis of the relaxation time τ = 0.08 obtained in course of the simulation (at the first approximation from the relation $2\pi f_{max}\tau \approx 1$), the frequency $f_{max} \approx 2$ Hz can be estimated, where the maximum of loss tangent should be observed.

5.4. Magnetic properties of the single-phase $BiFeO_{3-\delta}$ and $Bi_{0.9}La_{0.1}FeO_{3-\delta}$ perovskites

In order to study the effect of lanthanum on the magnetic properties of the $Bi_{1-x}La_xFeO_{3-\delta}$ multiferroics, the samples with non-stoichiometry δ weakly depending on the concentration x were selected. The samples with P = 400 MPa, in which δ decreases slightly from 0.08 for the $BiFeO_{3-\delta}$ to 0.07 for the $Bi_{0.9}La_{0.1}FeO_{3-\delta}$ (see Table 2), satisfy this condition. The behavior of the hysteresis $M(H)$ curves at the magnetization of the samples in a magnetic field up to H = 7 T testifies the availability of the ferromagnetic (FM) interactions in both samples (see Fig. 11). With increase in the La concentration from x = 0 to 0.1, the magnetization in the highest field 7 T decreases from M(7 T) = 0.9373 to 0.6669 emu/g at T = 4 K and increases from M(7 T) = 0.5842 to 0.6568 emu/g at T = 300 K (see Table 6). The coercive field of H_C increases both at a temperature T = 4 K from H_C = 1832 to 14664 Oe and at T = 300 K from H_C = 5392 to 11624 Oe. The residual magnetization of M_r increases from M_r = 0.04105 to 0.13221 emu/g at T = 4 K and from M_r = 0.04603 to 0.11866 emu/g at T = 300 K as well.

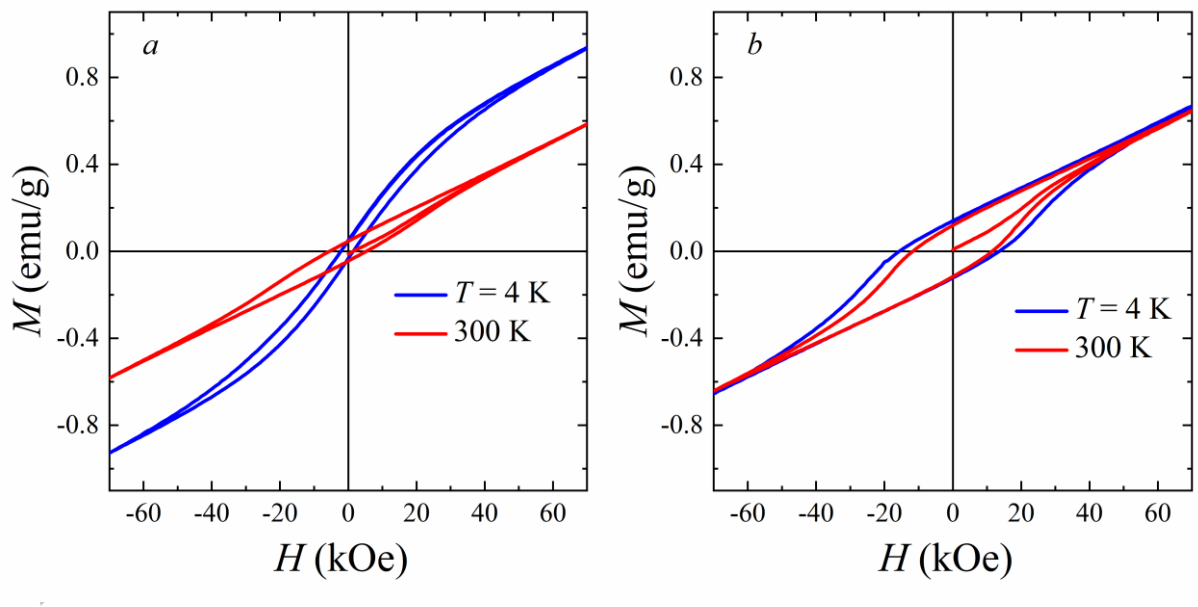

Fig. 11. Hysteresis curves of the $M(H)$ for the $BiFeO_{3-\delta}$ (*a*) and $Bi_{0.9}La_{0.1}FeO_{3-\delta}$ (*b*) in a magnetic field up to H = 7 T at temperatures of T = 4 and 300 K.

Table 6

Magnetic properties of the $Bi_{1-x}La_xFeO_3$ (P = 400 MPa) ceramics

x	H_C (Oe)		M_r (emu/g)		M(7 T) (emu/g)	
	4 K	300 K	4 K	300 K	4 K	300 K
0	1832	5392	0.04105	0.04603	0.9373	0.5842
0.1	14664	11624	0.13221	0.11866	0.6669	0.6568

An increase in the coercivity of the H_C and the change of magnetizations of the M(7 T) and M_r at the replacement of bismuth by lanthanum in the $Bi_{1-x}La_xFeO_3$ are a logical result which is caused by the destruction of the spin cycloid by lanthanum [23]. However, the appearance of ferromagnetism in the $BiFeO_{3-\delta}$ is an unexpected result and requires more detailed discussion. The residual magnetization M_r = 0.04105 emu/g in our sample $BiFeO_{3-\delta}$ at T = 4 K (see Table 6) is significantly ~ 70 times greater than M_r = 0.0006 emu/g for the same composition $BiFeO_3$, in which a cycloidal antiferromagnetism is observed [24]. The appearance of FM interactions in the pure $BiFeO_3$ can be caused by the appearance of the ferromagnetic $Fe_B^{2+} - O^{2-} - Fe_B^{3+}$ double exchange through oxygen between the Fe^{2+}($3d^6$, S = 2) and Fe^{3+}($3d^5$, S = 5/2) provided that Fe^{2+} ions are available in the B-positions of the perovskite [69]. The appearance of such FM clusters was observed in the $BiFeO_3$ films, in which FM ordering can be realized through a double-exchange of the Zener mechanism and is not associated to the Dzyaloshinskii-Moriya interaction [70]. A confirmation of this mechanism is the fact that the concentration of Fe^{2+} reaches 10 % (see Table 2) in the studied $BiFeO_{3-\delta}$ (P = 400 MPa) sample.

An absence of any anomalies in the $M_{ZFC}(T)$ and $M_{FC}(T)$ dependences (see Fig. 12) indicates a magnetic homogeneity and the absence of magnetic phase transitions in the temperature T = 2 – 400 K range. There is no discrepancy between the temperature dependences of the $M_{ZFC}(T)$ and $M_{FC}(T)$ magnetization (see Fig. 12). It means an absence of spin-glass behavior [71], and a phase separation of the magnetic subsystem in our samples regardless of the La content [72]. The magnetization M of all samples weakly varies over the whole temperature T = 2 – 400 K range and increases from M = 0.0020 –

0.0022 emu/g in a magnetic field H = 50 Oe to M = 0.58 – 0.68 emu/g in the H = 7 T. The sharp increase in the M_{ZFC} and M_{FC} magnetizations for the $BiFeO_{3-\delta}$ sample in the low-temperature region from 50 to 2 K (see Fig. 12 (*a*)) is due to the magnetic and spin heterogeneity [25, 73]. An absence of such a sharp increase in the M_{ZFC} and M_{FC} when $T \rightarrow 0$ in the $Bi_{0.9}La_{0.1}FeO_{3-\delta}$ sample (see Fig. 12 (*b*)) indicates its high magnetic purity, which once again confirms the magnetic homogeneity and correctness of the determined molar formulas of the real structure (see Table 2) with a low content of Fe^{2+} (5 %) in this sample.

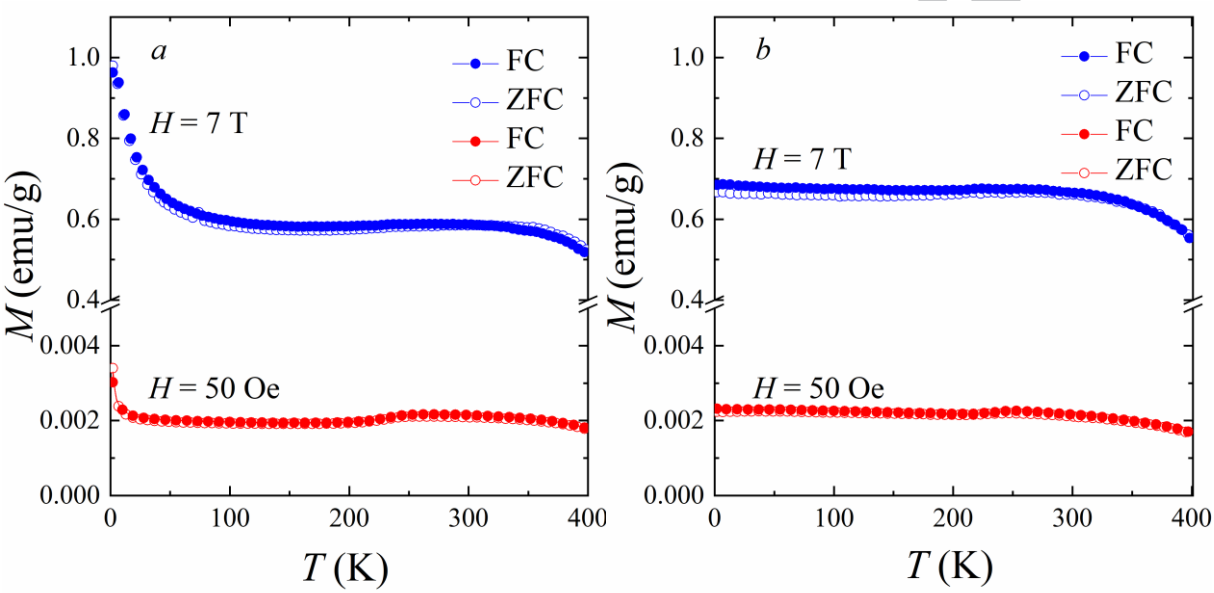

Fig. 12. The dependences of the $M_{ZFC}(T)$ and $M_{FC}(T)$ magnetization for the $BiFeO_{3-\delta}$ (*a*) and $Bi_{0.9}La_{0.1}FeO_{3-\delta}$ (*b*) in the magnetic fields of H = 50 Oe and 7 T.

Conclusions

X-ray diffraction, thermogravimetric, iodometric titration, SEM, XPS, dielectric spectroscopy and magnetic methods have been used for investigating the structure, microstructure, valence states, non-stoichiometry, dielectric and magnetic properties of the lanthanum-modified multiferroics obtained by the rapid liquid phase sintering method under different pressures P.

Taking into account the defect formation mechanism, the molar formulas of the real perovskite structure for the $BiFeO_{3-\delta}$ pure and lanthanum-doped $Bi_{0.9}La_{0.1}FeO_{3-\delta}$ bismuth ferrite have been determined. It has been found out that the real structure contains Bi^{3+}, Fe^{2+}, Fe^{3+}, O^{2-} ions as well as anion

$V^{(a)}$ and cation $V^{(c)}$ vacancies. Due to the low concentration of the $V^{(c)}$ vacancies, the deviation from stoichiometry in the cation sublattice can be neglected. The non-stoichiometry of the oxygen sublattice δ depends on the composition and the pressure *P* and can be varied in the range of δ = 0.07 – 0.22, which corresponds to a change in the concentration of the $V^{(a)}$ vacancies from 2.3 to 7.3 %. The SEM results confirm the chemical composition. The XPS data evidence valence state of ions in the single-phase $Bi_{0.9}La_{0.1}FeO_{3-\delta}$ multiferroics.

In the rapid liquid phase sintering method, the temperature regimes of rapid heating have been determined at a rate of 100 °C/sec (from room temperature to 770 °C) and 10 °C/min (from 770 to 850 °C) up to 850 ° C with a subsequent rapid cooling at a rate of 100 °C/sec down to room temperature for obtaining the single-phase $Bi_{0.9}La_{0.1}FeO_{3-\delta}$ multiferroics, whose composition corresponds to the concentration region of a destruction of the spin cycloid. It has been established that the concentration of Fe^{2+} from 27 to 5 % in the single-phase $Bi_{0.9}La_{0.1}FeO_{3-\delta}$ multiferroics by can be controlled by the changing pressure *P* from 200 to 400 MPa.

According to X-ray diffraction data, the crystal structure of the single-phase $Bi_{0.9}La_{0.1}FeO_{3-\delta}$ is a rhombohedrally *R*3*c* distorted hexagonal perovskite structure, the lattice parameters of which do not depend on the pressure *P*. Monotonic reductions in the lattice and volume of the unit cell while decreasing temperature from 290 to 18 K are observed without structure transformation.

According to the SEM data and dielectric spectroscopy, the crystal structure of the $Bi_{0.9}La_{0.1}FeO_{3-\delta}$ sample obtained under *P* = 200 MPa is small-porous with crystallite size ~ 1μm, which induces the accumulation of a charge at the crystallite boundaries and the appearance of colossal dielectric constant ε′ ~ $5\cdot10^5$ in the low-frequency range. In this sample, relatively large losses tanΔ ~ 1.5 are associated to increasing conductivity with the appearance of a ferromagnetic $Fe_B^{2+} - O^{2-} - Fe_B^{3+}$ double exchange. Increasing the pressure *P* up to 400 MPa reduces the crystallite size to ~ 450 nm and homogenizes the microstructure. Reducing non-stoichiometry δ from 0.18 to 0.07 decreases the concentration of Fe^{2+} from 27 to 5 % and lowers the initial dielectric constant. The initial dielectric constant of the $Bi_{0.9}La_{0.1}FeO_{3-\delta}$

multiferroics can be controlled and changed in ~ 5000 times from $\varepsilon' = 5 \cdot 10^5$ to 100 by variation of the pressure of the initial mixture of precursors from 200 to 400 MPa.

According to magnetic measurements, the magnetic structure of the $Bi_{0.9}La_{0.1}FeO_{3-\delta}$ single-phase multiferroics obtained by the RLS method is homogeneous with a large value of the coercitivity of $H_C \geq$ 10 kOe at room temperature. The magnitude of the magnetization and an absence of anomalies in its temperature dependence indicate the appearance of a weak ferromagnetism and the destruction of the spin cycloid in this sample by the lanthanum impurity.

Acknowledgements

This work was partially supported by Chinese Program “The Thousand Talents Program for Foreign Experts” of China (project WQ20162200339), State Scientific Research Program 2016-2020 "Physical materials science, new materials and technology" (subprogramme "Material Science and technology of materials", task No. 1.35) and Ministry of Education and Science of Russian Federation (award No. 3.6105.2017/8.9).

References

1. G. Catalan, J.F. Scott, Physics and Applications of Bismuth Ferrite, Adv. Mater. 21 (2009) 2463–2485.
2. N.A. Hill, Why Are There so Few Magnetic Ferroelectrics? J. Phys. Chem. B. 104 (2000) 6694–6709.
3. F. Matsukura, Y. Tokura, H. Ohno, Control of magnetism by electric fields, Nature Nanotechnology. 10 (2015) 209–220.
4. G. Le Bras, D. Colson, A. Forget, N. Genand-Riondet, R. Tourbot, P. Bonville, Magnetization and magnetoelectric effect in Bi1-xLaxFeO3 (0≤x≤0.15), Phys. Rev. B. 80 (2009) 134417.
5. A.A. Amirov, I.I. Makoed, Y.A. Chaudhari, S.T. Bendre, D.M. Yusupov, A.Sh. Asvarov, N.A. Liedienov, A.V. Pashchenko, Magnetocaloric Effect in BiFe1-xZnxO3 Multiferroics, J. Supercond. Nov. Magn. 31 (2018) 3283–3288.
6. Y. Guo, Y. Pu, C. Cui, J. Wan, C. Hui, Study of magnetodielectric effect and magnetic properties of BiFeO3-xBiYO3 ceramics, Materials Letters. 219 (2018) 190–193.
7. A.S. Panfilov, G.E. Grechnev, V.M. Ishchuk ,Effect of pressure on the magnetic properties of multiferroic BiFeO3, Low Temp. Phys. 41 (2015) 528–533.
8. C. Beekman, W. Siemons, T.Z. Ward, M. Chi, J. Howe, M.D. Biegalski, N. Balke, P. Maksymovych, A.K. Farrar, J.B. Romero, P. Gao, X.Q. Pan, D.A. Tenne, H.M. Christen, Phase Transitions, Phase Coexistence, and Piezoelectric, Adv. Mater. 25 (2013) 5561–5567.
9. G.L. Yuan, S.W. Or, Enhanced piezoelectric and pyroelectric effects in single-phase multiferroic Bi1-xNdxFeO3 (x=0–0.15) ceramics, Appl. Phys. Lett. 88 (2006) 062905-1–062905-3.
10. J.-H. Lee, M.-A. Oak, H.J. Choi, J.Y. Sonc, H.M. Jang, Rhombohedral–orthorhombic morphotropic phase boundary in BiFeO3-based, J. Mater. Chem. 22 (2012) 1667–1672.
11. A.P. Pyatakov, A.K. Zvezdin, Magnetoelectric and multiferroic media, Physics-Uspekhi. 55 (2012) 557–581.
12. F. Kubel, H. Schmid, Structure of a ferroelectric and ferroelastic monodomain crystal of the perovskite BiFeO3, Acta Cryst. 46 (1990) 698–702.
13. J.R. Teague, R. Gerson, W.J. James, Dielectric hysteresis in single crystal BiFeO3, Solid State Commun. 8 (1970) 1073–1074.
14. J.F. Li, J. Wang, N. Wang, F. Bai, B. Ruette, A.P. Pyatakov, M. Wuttig, R. Ramesh, A.K. Zvezdin, D. Viehland, Dramatically enhanced polarization in (001), (101), (111) BiFeO3 thin films due to epitiaxial-induced transitions, Appl. Phes. Lett. 84 (2004) 5261–5263.
15. J.G. Park, M.D. Le, J. Jeong, S. Lee, Structure and spin dynamics of multiferroic BiFeO3, J. Phys.: Condens. Matter. 26 (2014) 433202.
16. A.F. Popkov, M.D. Davydova, K.A. Zvezdin, S.V. Solov'yov, A.K. Zvezdin, Origin of the giant linear magnetoelectric effect in perovskitelike multiferroic BiFeO3, Phys. Rev. B. 93 (2016) 094435-1–094435-5.
17. I.A. Sergienko, E. Dagotto, Role of the Dzyaloshinskii-Moriya interaction in multiferroic perovskites, Phys. Reb. B. 73 (2006) 094434-1–094434-5.
18. I. Sosnowska, R. Przeniosło, Low-temperature evolution of the modulated magnetic structure in the ferroelectric, Phys. Rev. B. 84 (2011) 144404-1–144404-5.
19. A.K. Zvezdin, A.P. Pyatakov, Flexomagnetoelectric effect in bismuth ferrite, Phys. Status Solidi B. 246 (2009) 1956–1960.
20.Yu.F. Popov, A.M. Kadomtseva, S.S. Krotov, D.V. Belov, G.P. Vorob'ev, P.N. Makhov, A.K. Zvezdin, Features of the magnetoelectric properties of in high magnetic fields, Low Temp. Phys. 27 (2001) 478–479.
21. J. Ma, J. Hu, Z. Li, C.-W. Nan, Recent Progress in Multiferroic Magnetoelectric, Adv. Mater. 23 (2011) 1062–1087.
22. F. Huang, Z. Wang, X. Lu, J. Zhang, K. Min, W. Lin, R. Ti, Peculiar magnetism of BiFeO3 nanoparticles with size approaching the period of the spiral spin structure, Scientific Reports. 3 (2013) 2907.
23. V.S. Pokatilov, V.V. Pokatilov, A.S. Sigov, Local states of iron ions in multiferroics Bi1-xLaxFeO3, Phys. Solid State. 51 (2009) 552–558.

24. P. Suresh, S. Srinath, Observation of high coercivity in multiferroic lanthanum doped BiFeO3, J. Alloys Comp. 554 (2013) 271–276.
25. J. Lu, A. Gunther, F. Schrettle, F. Mayr, S. Krohns, L.P. Unkenheimer, A. Pimenov, V.D. Travkin, On the room temperature multiferroic BiFeO3: magnetic, dielectric and thermal properties, Eur. Phys. J. B. 75 (2010) 451–460.
26. Y. Li, X. Fang, M. Cao, Thermal frequency shift and tunable microwave absorption in BiFeO3 family, Scientific Reports. 6 (2016) 24837.
27. A. Maitre, M. François, J.C. Gachon, Experimental study of the Bi2O3–Fe2O3 pseudo-binary system, J. Phase Equilib. Diffus. 25 (2004) 59–67.
28. M. Thrall, R. Freer, C. Martin, F. Azough, B. Patterson, R.J. Cernik, An in situ study of the formation of multiferroic bismuth ferrite using high resolution synchrotron X-ray powder diffraction, J. Europ. Ceram. Soc. 28 (2008) 2567–2572.
29. M. Valant, A.-K. Axelsson, N. Alford, Peculiarities of a Solid-State Synthesis of Multiferroic BiFeO3, Chem. Mater. 19 (2007) 5431–5436.
30. M.S. Bernardo, T. Jardiel, M. Peiteado, A.C. Caballero, M. Villegas, Reaction pathways in the solid state synthesis of multiferroic BiFeO3, J. Europ. Ceram. Soc. 31 (2011) 3047–3053.
31. S.M. Selbach, M.-A. Einarsrud, T. Grande, On the Thermodynamic Stability of BiFeO3, Chem. Mater. 21 (2009) 169–173.
32. Y.P. Wang, L. Zhou, M.F. Zhang, X.Y. Chen, J.-M. Liu, Z.G. Liu, Room-temperature saturated ferroelectric polarization in BiFeO3 ceramics synthesized by rapid liquid phase sintering, Appl. Phys. Lett. 84 (2004) 1731–1733.
33. M. Kumar, K.L. Yadav, Rapid liquid phase sintered Mn doped BiFeO3 ceramics with enhanced polarization and weak magnetization, Appl. Phys. Lett. 91 (2007) 242901-1–242901-3.
34. L. Malavasi, Role of defect chemistry in the properties of perovskite manganites, J. Mater. Chem. 18 (2008) 3295–3308.
35. R.A. De Souza, M.S. Islamb, E. Ivers-Tiffe, Formation and migration of cation defects in the perovskite oxide, J. Mater. Chem. 9 (1990) 1621–1627.
36. M. Schrade, N. Maso, A. Perejon, L.A. Perez-Maqueda, A.R. West, Defect chemistry and electrical properties of BiFeO3, J. Mater. Chem. C. 5 (2017) 10077–10086.
37. A. Perejon, N. Murafa, P.E. Sanchez-Jimenez, J.M. Criado, J. Subrt, M.J. Dianez, L.A. Perez-Maqueda, Direct mechanosynthesis of pure BiFeO3 perovskite nanoparticles: reaction mechanism, J. Mater. Chem. C. 1 (2013) 3551–3562.
38. F. Yan, M.-O. Lai, L. Lu, Enhanced Multiferroic Properties and Valence Effect of Ru-Doped BiFeO3 Thin Films, J. Phys. Chem. C. 114 (2010) 6994–6998.
39. V.P. Pashchenko, A.A. Khor'yakov, A.V. Pashchenko, Yu.S. Prilipko, A.A. Shemyakov, Effect of oxygen nonstoichiometry on the structure, 55Mn and 57Fe NMR, electromagnetic properties, and magnetoresistance of manganese zinc ferrites, Inorganic Materials. 50 (2014) 191–196.
40. C.R. Hubbard, R.L. Snyder, RIR - Measurement and Use in Quantitative XRD, Powder Diffr. 3 (1988) 74–77.
41. I.V. Fesich, V.V. Trachevsky, A.G. Dziazko, S.A. Nedilko, A.K. Melnik, Optical and Electromagnetic Properties of $LaCoO_3$:Li^+; M^{2+} (M = Ca, Sr, Ba), J. Appl. Spectrosc. 81 (2014) 624–632.
42. A.V. Pashchenko, V.P. Pashchenko, V.K. Prokopenko, Yu.F. Revenko, Yu.S. Prylipko, N.A. Ledenev, G.G. Levchenko, V.P. Dyakonov, H. Szymczak, Influence of structure defects on functional properties of magnetoresistance (Nd0.7Sr0.3)1−xMn1+xO3 ceramics, Acta Materialia. 70 (2014) 218–227.
43. A.V. Pashchenko, V.P. Pashchenko, V.K. Prokopenko, V.A. Turchenko, Yu.F. Revenko, A.S. Mazur, V.Ya. Sycheva, N.A. Liedienov, V.G. Pitsyuga, G.G. Levchenko, Role of Structure Imperfection in the Formation of the Magnetotransport Properties of Rare-Earth Manganites with a Perovskite Structure, J. Exp. Theor. Phys. 124 (2017) 100–113.
44. A.V. Pashchenko, V.P. Pashchenko, N.A. Liedienov, V.K. Prokopenko, Yu.F. Revenko, N.E. Pismenova, V.V. Burhovetskii, V.Y. Sycheva, A.V. Voznyak, G.G. Levchenko, V.P. Dyakonov, H.

Szymczak, Structure, phase transitions, 55Mn NMR, magnetic and magnetotransport properties of the magnetoresistance La0.9−xAgxMn1.1O3−δ ceramics, J. Alloys Comp. 709 (2017) 779–788.
45. D. Briggs, M.P. Seach, Practical Surface Analysis, Auger and X-ray Photoelectron Spectroscopy: John Wiley&Sons, Chichester, New York, Brisbane, Toronto, Singapore, 1984.
46. Instruction Manual. Tesla. Q-Meter. BM 560. TESLA Brno, Nat. Corp., Brno CSSR. 1978, 107.
47. D.D. Tatarchuk, V.I. Molchanov, V.M. Pashkov, A.S. Franchuk, Microwave Dielectric Measurement Methods on the Base of the Composite Dielectric Resonator,// 2015 IEEE 35th International Conference on Electronics and Nanotechnology ELNANO-2015, April 21-24, 2015 Kyiv, Ukraine. – Kyiv: "Kyiv Polytecnic Institute", 2015, 231–234.
48. Y.K. Jeong, C.W. Bark, S. Ryu, J.-H. Lee, H.M. Jang, R3c-R3m Octahedron-tilting Transition in Rhombohedrally-distorted BiFeO3 Multiferroics, J. Korean. Phys. Soc. 58 (2011) 817–820.
49. P. Hermet, M. Goffinet, J. Kreisel, Ph. Ghosez, Raman and infrared spectra of multiferroic bismuth ferrite from first principles, Phys. Rev. B. 75 (2007) 220102.
50. J.B. Neaton, C. Ederer, U.V. Waghmare, N.A. Spaldin, K.M. Rabe, First-principles study of spontaneous polarization in multiferroic BiFeO3, Phys. Rev. B.71(2005) 014113-1–014113-8.
51. J.F. Scott, R. Palai, A. Kumar, M.K. Singh, N.M. Murari, N.K. Karan, R.S. Katiyar, New phase transitions in perovskite oxides: BiFeO3, SrSnO3, and Pb(Fe2/3W1/3)1/2Ti1/2O3, J. Am. Ceram. Soc. 91 (2008) 1762–1768.
52. R.D. Shannon, Revised effective ionic radii and systematic studies of interatomic distances in halides and chalcogenides, Acta Cryst. A. 32 (1976) 751–767.
53. M.T. Varshavskii, V.P. Pashchenko, A.N. Men', N.V. Suntsov, A.G. Miloslavskii, Defect Structure and Physicochemical Properties of Spinel Ferrites, Moscow: Nauka. 1988.
54. A.V. Pashchenko, N.A. Liedienov, V.P. Pashchenko, V.K. Prokopenko, V.V. Burhovetskii, A.V. Voznyak, I.V. Fesych, D.D. Tatarchuk, Y.V. Didenko, A.I. Gudymenko, V.P. Kladko, A.A. Amirov, G.G. Levchenko, Modification of multifunctional properties of the magnetoresistive La0.6Sr0.15Bi0.15Mn1.1-xBxO3-d ceramics when replacing manganese with 3d-ions of Cr, Fe, Co, Ni, J. Alloys Compd. 767 (2018) 1117–1125.
55. N.A. Razik, Frecise lattice constant determination of hexagonal, rhombohedral, and tetragonal crystals from X-ray powder diffractometric data, Phys. Status Solidi A. 90 (1985) K125–K128.
56. J.M. Moreau, C. Michel, R. Gerson, W.J. James, Ferroelectric BiFeO3 X-ray and neutron diffraction study, J. Phys. Chem. Solids. 32 (1971) 1315–1320.
57. R. Snyder, J. Fiala, H.J. Bunge, Defect and Microstructure Analysis by Diffraction, Oxford University Press, USA: 2000.
58. A.T. Kozakov, A.G. Kochur, K.A. Googlev, A.V. Nikolsky, I.P. Raevski, V.G. Smotrakov, V.V. Yeremkin, X-ray photoelectron study of the valence state of iron in iron-containing single-crystal (BiFeO3, PbFe1/2Nb1/2O3), and ceramic (BaFe1/2Nb1/2O3) multiferroics, J. Electr. Spectr. Related Phen.184(2011) 16–23.
59. T. Yamashita, P. Hayes, Analysis of XPS spectra of Fe2+ and Fe3+ ions in oxide materials, J. Appl. Surf. Science. 254 (2008) 2441–2449.
60. A.T. Kozakov, A.G. Kochur, L.A. Reznichenko, L.A. Shilkina, A.V. Pavlenko, A.V. Nikolsky, K.A. Googlev, V.G. Smotrakov, Single-crystal rare earths manganites La1−x−yBixAyMnO3±δ (A= Ba, Pb): Crystal structure, composition, and Mn ions valence state. X-ray diffraction and XPS study, J. Electr. Spectr. Related Phen. 186 (2013) 14–24.
61. M.F. Sunding, K. Hadidi, S. Diplas, O.M. Lovvik, T.E. Norby, A.E. Gunnæs, XPS characterisation of in situ treated lanthanum oxide and hydroxide using tailored charge referencing and peak fitting procedures, J. Electr. Spectr. Related Phen. 184 (2011) 399–409.
62. D.F. Mullica, C.K.C. Lok, H.O. Perkins, V. Young, X-ray photoelectron final-state screening in La(OH)3: A multiplet structural analysis, Phys. Rev. B. 31 (1985) 4039–4042.
63. K.S. Cole, R.H. Cole, Dispersion and Absorption in Dielectrics,J. Chem. Phys. 9 (1941) 341–351.
64. D.W. Davidson, R.H. Cole, The Dielectric Constant of Ethylene at High Pressures, J. Chem. Phys. 19 (1951) 1484–1490.

65. K. Majhi, B.S. Prakash, K.B.R. Varma, Extreme values of relative permittivity and dielectric relaxation in Sr2SbMnO6 ceramics, J. Phys. D: Appl. Phys. 40 (2007) 7128–7135.
66. S. Habouti, C.-H. Solterbeck, M. Es-Souni, UV assisted pyrolysis of solution deposited BiFeO3 multiferroic thin films. Effects on microstructure and functional properties, J. Sol-Gel Sci. Techn. 42 (2007) 257–263.
67. Z.X. Cheng, A.H. Li, X.L. Wang, S.X. Dou, K. Ozawa, H. Kimura, S.J. Zhang, T.R. Shrout, Structure, ferroelectric properties, and magnetic properties of the La-doped bismuth ferrite, J. Appl. Phys.103 (2008) 07E507-1–07E507-3.
68. C.G. Koops, On the Dispersion of Resistivity and Dielectric Constant of Some Semiconductors at Audiofrequencies, Phys. Rev. 83 (1951) 121–124.
69. K. Chakrabarti, K. Das, B. Sarkar, S. Ghosh, S.K. De, G. Sinha, J. Lahtinen, Enhanced magnetic and dielectric properties of Eu and Co co-doped BiFeO3 nanoparticles, Appl. Phys. Lett. 101 (2012) 042401-1–042401-5.
70. V.G. Prokhorov, G.G. Kaminsky, J.M. Kim, T.W. Eom, J.S. Park, Y.P. Lee, V.L. Svetchnikov, G.G. Levtchenko, Yu.M. Nikolaenko, V.A. Khokhlov, Evidence of non-Dzyaloshinskii–Moriya ferromagnetism in epitaxial BiFeO3 films, Low Temp. Phys. 37 (2011) 129–133.
71. C.-J. Cheng, C. Lu, Z. Chen, L. You, L. Chen, J. Wang, T. Wu, Thickness-dependent magnetism and spin-glass behaviors in compressively strained BiFeO3 thin films, Appl. Phys. Lett. 98 (2011) 242502-1–242502-3.
72. K.C. Verma, R.K. Kotnala, Tailoring the multiferroic behavior in BiFeO3 nanostructures by Pb doping, RSC Adv. 6 (2016) 57727–57738.
73. E.L. Fertman, A.V. Fedorchenko, D.D. Khalyavin, A.N. Salak, A. Baran, V.A. Desnenko, O.V. Kotlyar, E. Čižmár, A. Feher, E.S. Syrkin, A.I. Vaisburd, N.M. Olekhnovich, A.V. Pushkarev, Yu.V. Radyush, A. Stanulis, A. Kareiva, Multiferroic Bi0.65La0.35Fe0.5Sc0.5O3 perovskite: magnetic and thermodynamic properties, J. Magn. Magn. Mater. 429 (2017) 177–181.

Graphical abstract

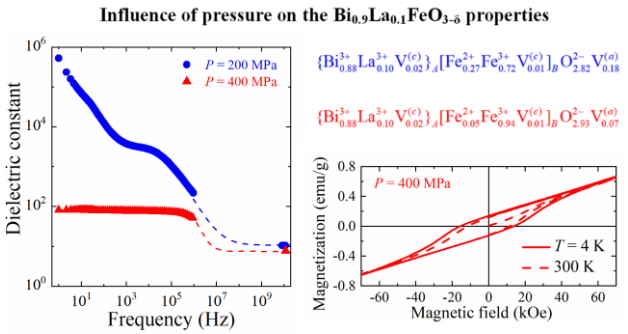

Highlights

1. Real molar formulas for $BiFeO_{3-\delta}$ and $Bi_{0.9}La_{0.1}FeO_{3-\delta}$ multiferroics were determined
2. Real structure contains Bi^{3+}, La^{3+}, Fe^{2+}, Fe^{3+}, O^{2-} ions and $V^{(a)}$, $V^{(c)}$ vacancies
3. Dielectric constant ε' reduces in 5000 times at 1 Hz with rising P from 200 to 400MPa
4. $Bi_{0.9}La_{0.1}FeO_{3-\delta}$ multiferroics show a large value of $H_C \geq 10$ kOe at room temperature
5. "Composition, Structure, Non-stoichiometry, Properties" correlation was established